Effect of Supercritical Friction Factor and Heat Transfer Model on the Stability of a Natural Circulation Driven Super Critical Water Reactor

M.A. van Iersel

Bachelor of Science Thesis

Delft University of Technology
Faculty of Applied Sciences
Dept. of Radiation Science and Technology
Sect. Nuclear Energy and Radiation Applications

Supervisor: Dr.ir. M. Rohde

Committee: Dr.ir. M. Rohde, TNW, TU Delft
Committee: Dr.ir. D. Lathouwers, TNW, TU Delft

Delft, January 2016

Abstract

The Super Critical Water Reactor (SCWR) is one of the six generation IV nuclear reactor designs. These designs were chosen as the most promising to deliver safe, sustainable and financially attractive nuclear reactors. The SCWR uses water as coolant and operates with temperatures up to 500 °C. These high coolant temperatures allow the SCWR to reach a much higher thermal efficiency (up to 45%) compared to other water cooled nuclear reactors. Several designs to build a SCWR have been proposed, among them the European High Performance Light Water Reactor (HPLWR). After this design was published it was proposed to drive the flow in the reactor by natural circulation, using the large density differences within the system, instead of a conventional pump(Rohde et al., 2011).

To investigate the feasibility of this idea, the NERA group in Delft built a scaled loop mimicking the HPLWR, called DeLight (Delft Light Water Reactor). After the experiment, Spoelstra(2012) adjusted a 1-D computational model(Kam, 2011) to capture the physics of flow instabilities in the experimental facility. However, the predictions from the experiments did not entirely agree with the stability data obtained with the model. The goal of this research is to implement a supercritical friction factor correlation and heat transfer model into the existing model made by Spoelstra. Then a new stability analysis is done and compared to the existing benchmark data. Before adjustments to the model are made, the available supercritical friction factor and Nusselt number correlations found in literature are assessed and an analysis is made of their behavior during supercritical heating/cooling. After the analysis a friction factor model proposed by Fang et al.(2012) as well as a Nusselt correlation proposed by Mokry et al.(2009), are implemented in the model. Steady-state simulations showed good agreement between the experimentally measured mass-flow rates and predicted values with the adjusted model. This indicates the new friction model accurately describes the friction distribution in the system. Although the stability analysis yielded a neutral stability boundary that does not accurately describes the experimental findings, the approximation is better than both Spoelstra and Schenderling. Also, the effect of the Nusselt number correlation on system stability turned out to be significant. The friction factor model also influences stability, but the effects are much smaller that the influence the Nusselt correlation has. It is concluded more comprehensive measurements and modeling should be done to better understand the variables within the system, especially the Nusselt number, that affect the stability of the system.

Contents

Chapter 1

introduction

1.1 iv Generation Nuclear Reactors

Nuclear energy has been around since the 1960s and has provided a significant part of the world's electrical energy demand since. After a strong rise between 1970 and 1990 nuclear energy has fallen out of favor due to large calamities such as Chernobyl and, twenty years later, Fukushima. This distrust toward nuclear energy and technology has made safety a top priority among scientists and engineers working on new nuclear reactors and applications. This was no different in the generation IV international forum, where six nuclear reactor designs were proposed. The aim of this forum is to bundle the efforts of industrial and academic partners toward sustainable, inherently safe, economically viable nuclear reactors. One of these six reactor types is the Super Critical Water Reactor (SCWR)(see figure 1.2). This Reactor operates under high temperature and pressure so that the water becomes supercritical, hence the name.

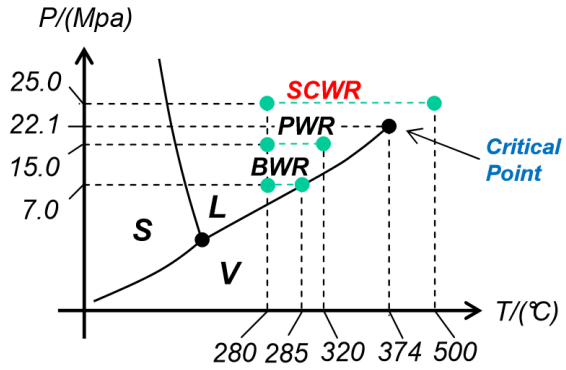

Figure 1.1: Phase diagram of water, the operating ranges of the different LWR's are shown. Note that the SCWR by far has the widest range and is the only one phase system. (Source: Spoelstra, 2012)

One of the key advantages of operating with a coolant in supercritical state is that this makes the reactor a one phase system(see figure 1.1). Around the pseudo-critical point, the point where the supercritical fluid experiences the transition from liquid-like to gas-like state, several properties change significantly but no phase shift occurs. This means the core outlet temperature is not limited by a boiling point, which is the case for a Pressurized Water Reactor (PWR) for example. In the SCWR the outlet temperature is only limited by the material temperature limit, which is much higher (roughly 620 °C for the HPLWR

design). This allows for feasible operating temperatures of up to 500 °C. Reactor efficiency is directly related to core outlet temperature, i.e. the thermal efficiency depends on the temperature difference between the reactor core and the condenser temperature. Because the environment is usually used as a heat sink the condenser temperature is fixed at 10-20 °C, this means a higher core outlet temperature results directly in higher thermal efficiency. This makes the SCWR economically a very interesting concept. Where Boiling Water Reactors (BWR) usually have an effective efficiency of 33% the SCWR has a projected efficiency of 45%. Although the SCWR operates at very high pressure (250 bar), which is structurally demanding, the construction costs are relatively low. Because the SCWR is a one phase system, no phase separation equipment, as found in the BWR, is necessary. Furthermore, supercritical water can directly drive the turbine because of the density drop around the pseudo-critical point. The required turbines have already been developed, e.g. (Viswanathan, 2005), and are being used in fossil fuel plant, driving down further development cost.

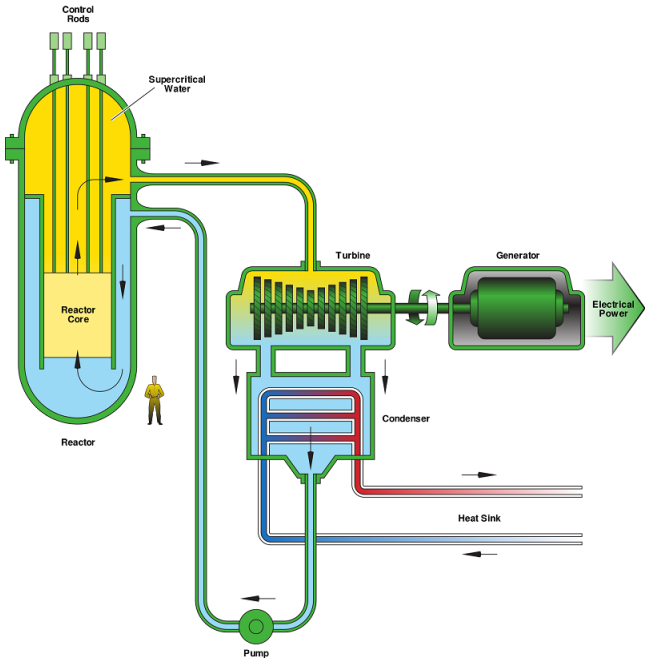

Figure 1.2: General design of SCWR. Note that the reactor does not need a secondary cycle, the supercritical water directly drives the turbine. (Source: Spoelstra, 2012)

1.2 HPLWR

Several Generation IV international partners have proposed SCWR designs, among them is the European High Performance Light Water Reactor (HPLWR). The fuel elements used in this reactor design are developed by Hofmeister et al. (2007) and use conventional uranium-oxide and MOX fuel. The fuel is placed in clusters(see figure 1.3a) so the coolant water can flow through the channels between the fuel bundles. The coolant water is heated from roughly 280 °C to 500 °C at 250 bar. Because the flow rate is not constant in every channel, for instance due to manufacturing uncertainties, there is a chance of hotspots within the core. This can cause structural limits to be exceeded. Schulenberg et al. (2008) proposed a way to reduce this effect by slitting the HPLWR core into three segments with mixing chambers in-between the core sections(see figure 1.3c). This solution reduces the temperature differences

between the channels below the point where structural limits would be exceeded. Each core section, being the evaporator and super heaters I and II, house 52 fuel bundles.

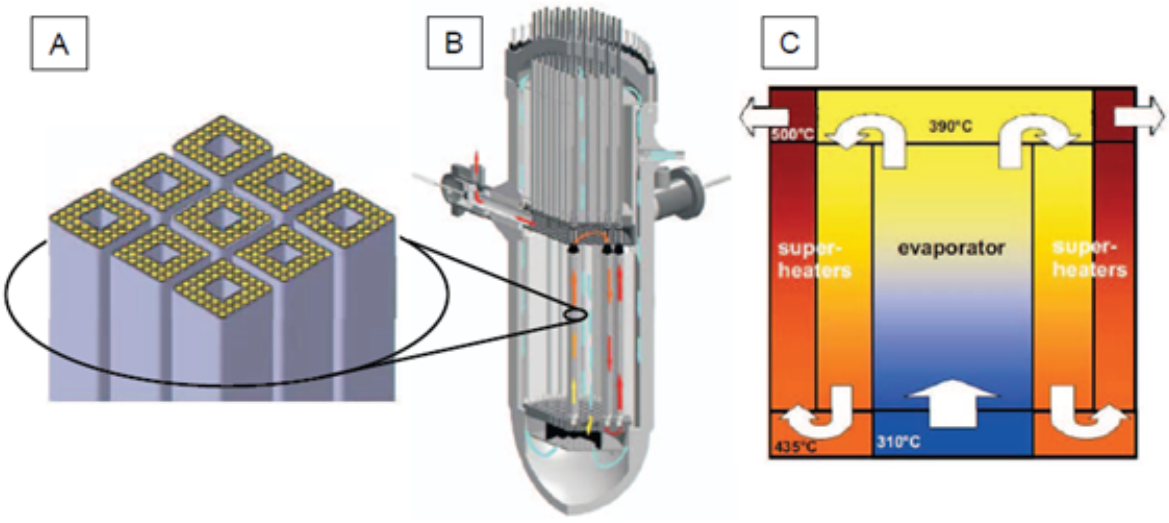

Figure 1.3: Nine fuel assemblies in a cluster(a) and representation of three pass core proposed in the HPLWR(b,c) (Scource: Hofmeister et al. (2007); Ortega Gómez (2009); Schulenberg et al.(2008))

Besides its function as coolant, the water in the HPLWR also has the function of neutron moderator. The function of a moderator in a nuclear reactor is to reduce the energy level of the neutrons released in the fission reactions to a lower level so the neutron can potentially initiate a new fission reaction. The degree of moderation depends on the density of the water in the core section, high density means more moderation and thus more fission reactions and vice versa. Because the coolant water has a large difference in density as it heats up, 780 kg/m3 to 90 kg/m3, the moderating abilities heavily depend on core section, i.e. coolant temperature. The loss of moderation is compensated with by relatively cold feedback water through the square channels in the reactor core (see figure 1.3b). This water mixes with the core inlet coolant at the evaporator entrance.

An interesting idea to make nuclear reactor inherently safe is natural circulation. This means the coolant will flow without a mechanical pump. This idea is not new, e.g. the BWR in Dodenwaard has been a natural circulation driven reactor. The idea of natural circulation is based on a density difference between the downcomer and riser. The HPLWR has a large density difference between the riser and the downcomer and therefore could be designed so that natural circulation is sufficient to cool the core, making the reactor inherently safe. The riser is required to produce enough driving force. The current general plans for the HPLWR do not include a natural circulation driven design, however the implementation of natural circulation to the HPLWR design has been investigated. This research will be discussed later in this chapter.

1.3 Supercritical Fluid Properties and Stability

Because the SCWR operates with a coolant in supercritical state, it is very important to understand the behavior of fluids under these conditions. Although the coolant does not experience a phase change, there are significant changes in properties within the reactor core. Every supercritical substance has a pseudo-boiling point at which a transition in properties takes place, the so-called pseudo-critical point (See figure 1.4). This pseudo-critical point divides the liquid-like phase and the gas-like phase and fluid properties such as density, viscosity, heat capacity and thermal conductivity change dramatically. The effects on the mass-flow and heat transfer within the reactor are complex, especially when the reactor is driven by natural circulation.

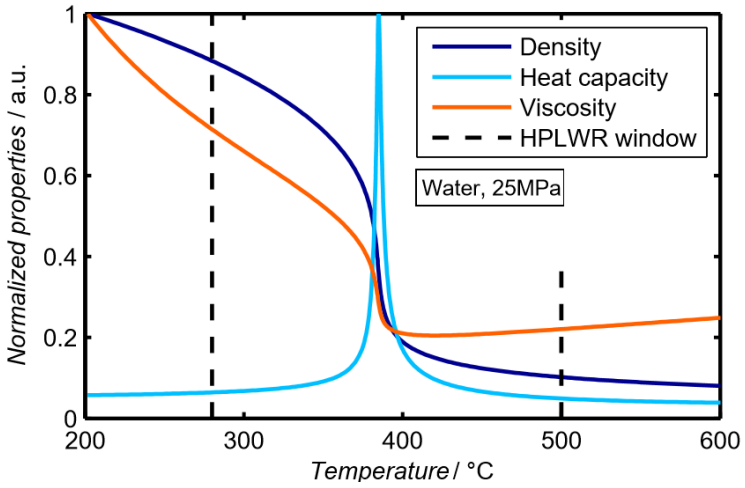

Figure 1.4: Properties of supercritical water around the pseudo-critical point, 384.90 °C at 250 bar. The operating window of the HPLWR is indicated with the dotted line. (Source: Spoelstra, 2012)

Flow instabilities occur all the time in a complex, turbulent system such as a nuclear reactor. How the system responds to these disturbances is what makes the reactor either stable or unstable. There are several instabilities that can occur within channel flows(Ambrosini, 2007; Ortega Gómez, 2009), typically divided in two categories; static and dynamic instabilities(Boure et al., 1973). An example of static instability are Leginegg instabilities(Fukuda and Kobori, 1979). This type of instability occurs when the system has more than one steady-state solution, the flow rate can alternate between these solutions in a non-periodic manner. Although the alternation between several solutions is non-periodic, steady-state channel analysis can predict unstable working points. Leginegg instabilities will not be studied further in this thesis.

Where steady-state analysis can predict the unstable working point for static instabilities, dynamic instabilities require transient analysis for proper prediction. Dynamic instabilities are the reaction of the flow to small perturbations and, when a positive feedback mechanism is in place, can grow significantly over time thus disrupting the system. A well-studied type of dynamic instability is the Density Wave Oscillation (DWO)(e.g.; March-Leuba and Rey, 1993). DWOs are common in BWR due to the large density differences throughout the system. The density within the HPLWR also changes significantly within the core, thus making DWOs a likely occurrence. DWOs are created when mass-flow fluctuations move through the core, the area's of lower mass-flow will spent more time in the core thus

becoming hotter and less dense than the faster flowing areas which will be colder and denser. The result of these fluctuations is a sinusoidal DWO traveling through the system.

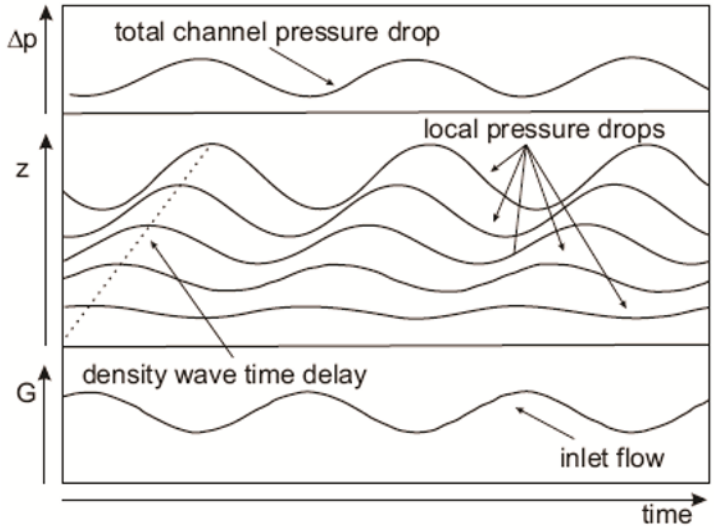

Figure 1.5: Example of type II instability; density wave oscillations in the core. If the inlet flow and pressure drop are 180 degrees out of phase, the perturbation grows maximally. (source: Ortega Gómez, 2009)

The DWO affect several variables within the system, for instance the gravitational pressure drop and thus the driving force of the natural circulation. These instabilities can reinforce each other, i.e. induce a positive feedback, when the core inlet mass-flow and the gravitational pressure drop are out-of-phase with respect to each other. This type of instability is labeled a type I instability. Type I instabilities manifest themselves over the length of the core and the riser while type II instabilities take place only in the core. Type II instabilities can also be caused by DWO, this time a feedback mechanism by the frictional pressure drop over the core (see figure 1.5). Positive feedback is achieved when the DWO and the frictional pressure drop are 180 degrees out of phase. The frequency of Type II instabilities is higher than that of type I instabilities due to the relatively short transit time in the core.

Because the coolant in the HPLWR is also the moderator, a change in density causes a change in moderation as well. The low density areas of the DWO causes fewer neutron to start a new reaction while a higher density area achieves the opposite. DWO can thus cause an oscillation in core power, this in turn influences the density in the core. These effects can also reinforce each other, rendering the system unstable.

1.4 Literature Survey

In 2012, T'Joen and Rohde published an article concerning an experimental study of a natural circulation driven supercritical cooling loop, simulating a SCWR(T'Joen and Rohde, 2012). In this article a comprehensive study was lain out about the stability of such a loop, serving as benchmark data for stability analysis exploring the possibility of a natural circulation driven SCWR. The facility was given the name Delft Light Water Reactor, or short DeLight, and the design was based on HPLWR. R23 (Freon) was used as coolant to reduce structural requirements, the scaling rules were derived(Rohde et al., 2011). The system operates under 57 bar with temperatures from -40 to 110 °C. Neutronic feedback was implemented into the

electrical heating to mimic a real reactor. A division between stable and unstable points was made by measuring the decay ratio after applying a small perturbation. The results of these measurements is the neutral stability boundary (see figure 1.6). This line separates the stable operating conditions from the unstable operating conditions. N_{SUB} and N_{PHC} are dimensionless numbers based on system properties.(T'Joen and Rohde, 2012)

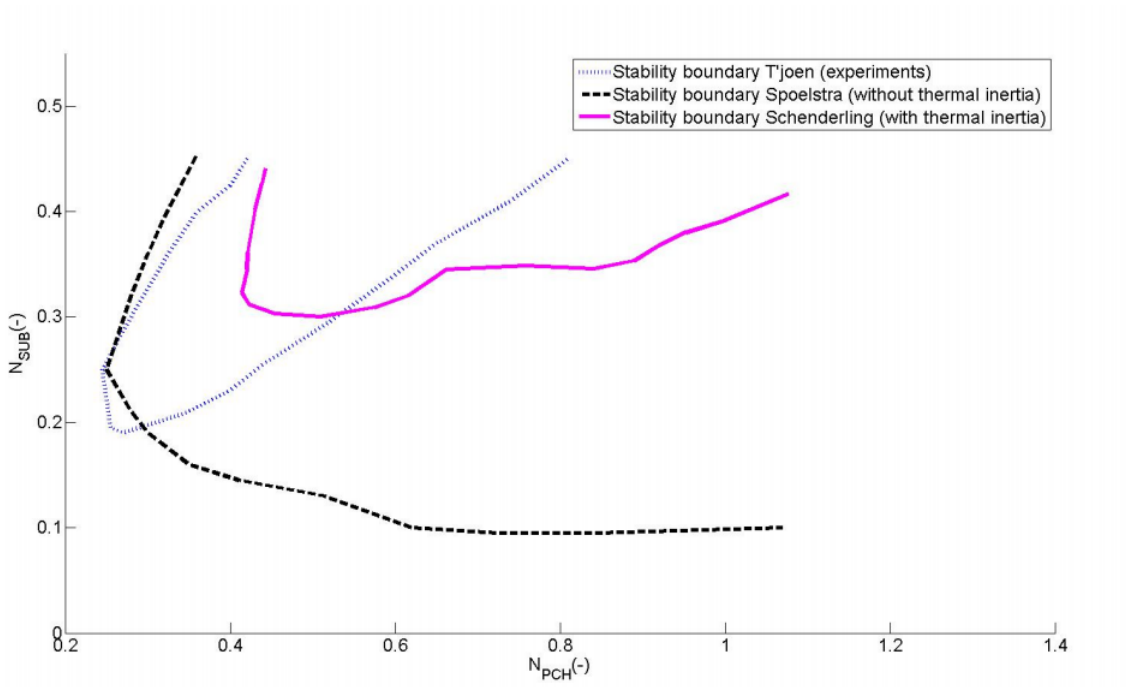

Figure 1.6: Neutral stability boundary as found by T'Joen and Rohde in the DeLight experiments and the computational simulations from Spoelstra and Schenderling. N_{SUB} and N_{PHC} are dimensionless numbers representing operation points of the DeLight(T'Joen and Rohde, 2012). (Source: Schenderling, 2013)

After the DeLight experiments, J. Spoelstra wrote a 1-D model to represent the physical phenomenon that take place within the DeLight facility.(Spoelstra, 2012) The model is based on the numerical model from Kam (2011) and implements the Stealth code(Koopman, 2008) which was originally meant for a boiling system. Spoelstra's model yielded a neutral stability boundary similar to the experiments for low power, however higher power results did not agree(see figure 1.6). Several assumptions and simplifications were made by Spoelstra such as the lack of thermal inertia in the structure and a friction and heat transfer model developed for supercritical fluids. With these simplifications in mind, Schenderling implemented thermal inertia to the model to explore its effect on the neutral stability boundary. Although the results are better for high powers, they still differ from the experimental findings as figure 1.6 shows.

1.5 Thesis Objectives and Outline

The objective of this thesis is to explore the effect of the implication of a supercritical friction factor correlation and heat transfer model on the stability analysis of a natural circulation driven supercritical water Reactor. The starting point of this thesis will be the work done

by Schenderling and Spoelstra, trying to capture the physics of the experimental DeLight facility in a computational model. First, an assessment will be made of current supercritical friction and heat transfer models. These models will be compared with each other and the current friction and heat transfer model used in the code. Thereafter one or several models for both the frictions factor and the heat transfer coefficient will be chosen for implementation into the code. After implementation the new model will be compared to the Schenderling and Spoelstra code through steady-state and transient analysis. Ultimately, a new neutral stability boundary will be computed.

The outline of this thesis follows as; After this introduction chapter the DeLight experiment will be discussed in chapter 2. Chapter 3 assesses the current friction factor correlation in the model and surveys the available supercritical friction factor models from literature. Chapter 4 than discusses the heat transfer model in a similar manner. The experimental procedure is discussed in chapter 5 after which chapter 6 takes a closer look at the behavior of several correlations during supercritical heating/cooling. Chapter 7 introduces and discusses the results of this thesis, flowed by the conclusions and outlook in chapter 8.

Chapter 2

DeLight Setup

In this chapter the DeLight experiment(T'Joen and Rohde, 2012) will be discussed. Section 2.1 gives an overview of the geometry and components. Section 2.2 discusses the experimental procedure.

2.1 Geometry and Components

To explore the possibility of a natural circulation driven HPLWR the DeLight facility was built(T'Joen and Rohde, 2012). This facility is designed as a scaled model of the HPLWR with the goal of studying the stability of such a reactor. To reduce the structural requirements the coolant in the DeLight facility is not water which operates between 280 and 500 °C, at 250 bar. Instead, Freon R23 was chosen as the coolant with its operating temperature between -30 and 100 °C. The scaling rules where derived by Rohde et al. (2011). Figure 2.1 is a schematic representation of DeLight. To better capture the facility, the riser and the downcomer are not fully displayed, i.e. they are much longer in the real setup.

As in the HPLWR, the core consist of three segments, the evaporator, super heater I and super heater II. The segments are 80 cm stainless steel pipes with an inner diameter of 6 mm and a thickness of 0.5 mm. The core is heated by sending a very high current through the pipes supplied by Delta SM15-200 power units and can be controlled per core section via the voltage. The total power is distributed over the three core sections following the same distribution as the HPLWR, 53% in the evaporator, 30% in superheater I and 17% in superheater II. The largest power that can be supplied to the system is 18 kW. The core neutronics of the HPLWR are taken into account as well. τ, an adjustable time constant, is the amount of time is takes for feedback to occur. In this thesis τ was always set to 6 seconds.

After the core the R23 reaches the riser. The tubing in the riser and downcomer has an inner diameter of 1 cm. The transition from core diameter to riser/downcomer diameter is a gradual contraction/expansion over the length of three centimeters. The turbine and condenser are modeled as two heat exchangers in series and act as heat sink to the system. The first heat exchanger is fed with the building water supply and is able to absorb much more heat than is required which causes the outlet temperature of the first heat exchanger to be constant at 17 °C. This means the transition from gas- to liquid-like-state always happens in the first heat exchanger. The second heat exchanger reduces the temperature to the desired point. To reduce heat losses most sections are isolated with 25 mm of Armacell.

The core and preheater however are not isolated. To ensure an operating pressure of 57 bar, the buffer was added to the system. The buffer system works via a prison(Parker Series 5000 Piston Accumulator), e.g. at higher pressures the buffer vessel will grow larger decreasing the pressure and vice versa.

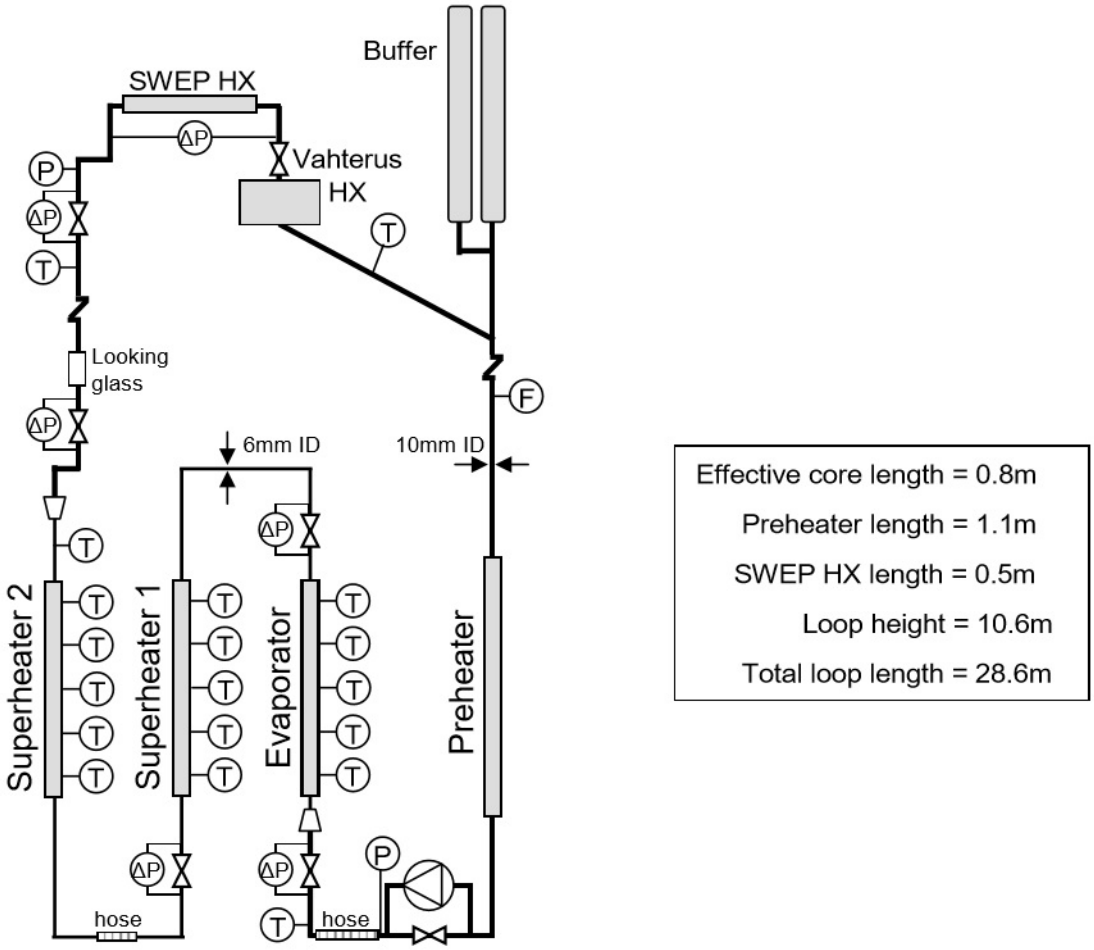

Figure 2.1: Schematic representation of the DeLight facility, for precise measurements see Appendix A. (Scource: Spoelsta, 2012)

The DeLight facility contains a large number of sensors. Bulk temperature is measured throughout the facility and in five different points in each core section. Absolute pressure is measured at the top and the bottom of the installation and the pressure drop (Δp) throughout the system. The F symbol at the downcomer indicates a flow meter. The measured values are also connected to a safety control which shuts down the facility if limits are exceeded.

2.2 Measurements

In order to produce a set of stability benchmark data, measurements were conducted. Each measurement started by reaching a steady-state working point. This was done by starting the

flow with an electrical pump while gradually adding power to the core segments, heating up the system. When steady-state is reached the core temperature, and thus density, is measured before turning on the neutronic feedback. When the feedback turned on, the measurement began. Depending on the stability of the working point the density and neutronic oscillations will either grow or dampen over time. To determine whether a point is stable or unstable the decay ratio is calculated using a fitting function, equation (2.1), to the first two periods of the auto-correlation function(Marcel, 2007; T'Joen and Rohde, 2012). The following expression (2.2) then yields the decay ratio.

$$y = a_0 + (1 - a_0 - a_1)e^{b_1\tau} + a_1 e^{b_2\tau} cos(\omega\tau) \tag{2.1}$$

$$DR = e^{\frac{2\pi b_2}{|\omega|}} \tag{2.2}$$

The decay ration indicates whether a perturbation grows or decays over time, i.e. $DR > 1$ indicates a growing perturbation and $DR < 1$ a decaying perturbation. At $DR = 1$ the perturbation does not change over time. When a point was determined unstable the signal was measured until the fluctuation exceeded 10% of the initial power, this power fluctuation occurred due to the neutronic feedback. When a point was deemed stable and no large oscillations were present, the power was increased by 250-500 W for 5 seconds. Then the decay of this large perturbation was measured until it became indistinguishable.

Chapter 3

Supercritical Friction Factor Model

This chapter will discuss the friction factor. First, in section 3.1, the current friction model is assessed. Section 3.2 explains why a supercritical friction factor models could improve model performance and section 3.3 discusses several friction factor correlations found in literature.

3.1 Current Friction Factor Model

The current method to calculate the friction between the wall and flow is a combination of several isothermal friction factor correlations. Which correlation is used, depends on the Reynolds number at that point in the simulation. The used correlations are shown below. All these equations accurately describe subcritical flow in their respective Reynolds windows.

$$Poisseuille \qquad f = \frac{64}{Re} \qquad Re < 2000 \tag{3.1}$$

$$Blasius \qquad f = 0.316 Re^{-0.25} \qquad Re < 30.000 \tag{3.2}$$

$$McAdams \qquad f = 0.184 Re^{-0.20} \qquad 30.000 < Re < 10^6 \tag{3.3}$$

$$Haaland \qquad f = (-1.8 \log_{10} \left[\frac{\epsilon}{3.7D}^{\frac{10}{9}} + \frac{6.9}{Re} \right])^{-2} \qquad 4.000 < Re < 10^8 \tag{3.4}$$

Here Re is the Reynolds number, D the hydraulic dynamiter and ϵ the surface roughness. Effectively, Haaland is mainly used during the stability analysis. The friction factor has a large effect on the steady-state mass-flow rate as the average shear wall stress $\tilde{\tau_w}$ is modeled according to Darcy's definition (3.5)(Todreas and Kazimi, 1989).

$$M = A\sqrt{\frac{8\tilde{\tau}_w \rho}{f}} \tag{3.5}$$

Here M is the mass-flow, ρ the dencity and A the contact surface.A supercritical friction factor model may also effect the stability of the system, namely the feedback between a DWO and the friction pressure drop in the core. When the friction factor increases or decreases with a change in density this will influence the size of the perturbation, either positively or negatively.

3.2 Failures of Current Model

Although the current friction factor model can accurately describe liquid state, there are severe errors when applied to a supercritical flow. Supercritical flow is complex, especially around the pseudo-critical point. The system properties change tremendously and so the transition between the liquid-like and gas-like state is often referred to as pseudo-boiling. In the DeLight facility the heat enters the bulk via the heated pipes representing the core. This means the temperature of the pipe must be higher than the bulk temperature causing an extremely thin layer of fluid, dx, to have the same temperature as the pipes. When the bulk temperature is close to the pseudo-critical point, the properties of the hotter layer near the wall can be significantly different than bulk properties. This effect is called pseudo-film boiling. This is very similar to the subcritical film boiling and dry-out boiling, where gas bubbles forming near the wall influence flow turbulence, heat transfer and shear wall stress. In BWR's and PWR's respectably dry-out and film boiling play a large role and pseudo-film boiling should be accounted for in the SCWR as well.

Generally, experiments have determined that the friction factor of a supercritical substance is higher when the substance is being cooled and lower while heating, due to pseudo-film boiling(Fang et al., 2012).

3.3 Choice of a New Friction Factor Model

Several experimental correlations have been proposed to capture the behavior of the friction factor of a supercritical flow. Fang et al. (2012) made an assessment of current models and combined the existing experimental data to produce a new correlation that is not specific to one fluid and has lower relative errors than the existing models. The evaluation of the available models and experimental data is captured in table 3.1.

Three of the available correlations have been chosen for further assessment; the Fang, Yamashitah and Popov correlations. This choice is based on their performance in the study and the possibility of implementation in the DeLight model, considering the available and known variables within the model. For instance, the Petrov and Popov(1988) correlation requires the acceleration factor(Fang et al., 2012) to be calculation. This causes the implementation of this correlation in the DeLight model to be much more complicated compared to the other available correlations. It should be noted however, that all of the studies used different fluids than R23 and most correlations are based on experiments with only one fluid. This makes it extremely difficult to determine what friction factor correlation is best and thus how well the behavior in the DeLight facility is modeled.

Table 3.1: Overall weighted error of most-used models per substance/all data. The mean absolute relative deviation(MARD) and mean relative deviation(MRD) are given for every substance/all data. A, b, c, represent the percentage of date points that have a smaller absolute relative deviation of respectably, 10, 20, 30 percent. (Source: Fang et al., 2012)

	Correlation	New correlation	Yamashitah	Petrov–Popov (1988)	Andresen–Garimella	Popov	Petrov–Popov (1985)	Isothermal smooth
All Data	MARD	**17.6**[d]	**19.5**	**20.1**	**18.3**	**21.6**	**37.0**	**25.9**
	MRD	−4.9	−7.1	−13.0	4.9	−15.5	14.5	−20.1
	[a]	30.0	28.5	28.7	40.5	24.1	21.0	20.5
	[b]	64.9	59.0	52.1	63.9	48.7	49.2	38.2
	[c]	82.1	81.0	79.2	79.2	76.2	68.7	65.6
R410A	MARD	**17.5**[d]	**19.5**	**20.9**	**17.3**	**22.1**	**37.7**	**27.0**
	MRD	−5.1	−7.7	−15.9	1.6	−18.5	18.1	−25.2
	[a]	36.1	32.7	28.5	38.8	26.6	24.0	18.6
	[b]	64.6	60.1	52.9	66.5	51.0	51.3	40.3
	[c]	79.5	79.1	75.3	82.9	71.1	65.8	63.8
R404A	MARD	**18.6**[d]	**23.2**	**19.8**	**6.9**	**23.6**	**58.1**	**29.4**
	MRD	−13.2	−7.2	−19.5	−5.9	−22.1	32.4	−29.4
	[a]	13.3	11.1	22.2	80.0	2.2	8.9	0.0
	[b]	73.3	44.4	37.8	97.7	20.0	42.2	0.0
	[c]	84.4	80.0	91.1	100.0	88.9	73.3	53.3
CO_2	MARD	**19.0**[d]	**18.1**	**16.9**	**26.2**	**17.1**	**19.9**	**16.3**
	MRD	0.2	−3.7	−5.9	19.5	−5.5	0.9	−8.3
	[a]	9.4	20.3	31.3	29.7	29.7	18.8	42.2
	[b]	56.3	59.4	59.4	42.2	59.4	50.0	54.7
	[c]	89.1	85.9	89.1	54.7	89.1	84.4	84.4
R22	MARD	**12.5**[d]	**14.7**	**21.0**	**34.1**	**26.1**	**35.8**	**36.4**
	MRD	0.7	−10.6	20.0	28.1	9.1	−33.7	36.2
	[a]	55.6	38.9	38.9	5.6	22.2	16.7	22.2
	[b]	77.8	77.8	50.0	16.7	50.0	33.3	44.4
	[c]	88.9	94.4	72.2	61.1	72.2	44.4	55.6

[a] Percentage of data points within the RD of ±10%.
[b] Percentage of data points within the RD of ±20%.
[c] Percentage of data points within the RD of ±30%.
[d] A bold line is the first line of the given data group.

3.3.1 Fang et al. (2012)

The friction factor correlation produced by Fang et al. is a combination of the existing data and correlations. The goal was to reduce errors overall and obtain a generally applicable correlation.

$$f = f_{iso,b}\left(\frac{\mu_w}{\mu_b}\right)^{0.49\left(\frac{\rho_f}{\rho_{pc}}\right)^{1.31}} \tag{3.6}$$

$$f_{iso,b} = 1.613\left[0.234\left(\ln\left(\left(\frac{\epsilon}{D}\right)^{1.1007} - \frac{60.525}{Re^{1.1105}} + \frac{56.291}{Re^{1.0712}}\right)\right)\right]^{-2} \tag{3.7}$$

An interesting observation can be made regarding the correlation. When the wall temperature is equal to the bulk temperature the term $(\frac{\mu_w}{\mu_b})$ becomes 1 and the friction factor becomes isothermal. This makes sense since pseudo-film boiling will no longer be an issue.

3.3.2 Yamshitah et al. (2003)

Yamashita et al. (2003) experimentally investigated the friction factor using supercritical R22 flowing through a uniformly heated vertical pipe with a diameter of 4.4 mm. This correlation also has a supercritical term where $(\frac{\mu_w}{\mu_b})$ becomes 1 if the relative temperature between wall and bulk is zero.

$$f = f_{iso,b}(\frac{\mu_w}{\mu_b})^{0.72} \tag{3.8}$$

$$f_{iso,b} = \frac{0.314}{0.7 - 1.65\log Re + (\log Re)^2} \tag{3.9}$$

3.3.3 Popov (1967)

A correlations was found by Popov in 1967 by investigating turbulent flows of supercrtitical CO_2 cooling. $f_{iso,b}$ is calculated with the Filonenko equation. The supercritical term in this correlation is based on the changes in density rater than viscosity, which is the case for the two previous correlations. The correlation also has a supercritical term where, in this case, $(\frac{\rho_f}{\rho_b})$ becomes 1 if the relative temperature between wall and bulk is zero.

$$f = f_{iso,b}(\frac{\rho_f}{\rho_b})^{0.74} \tag{3.10}$$

$$f_{iso,b} = (0.79\ln Re - 1.64)^{-2} \tag{3.11}$$

Chapter 4

Heat Transfer Model

This chapter takes a closer look at the heat transfer modeling in the DeLight model. Section 4.1 discusses the heat transfer model used by Spoelsta. Then, in section 4.2, the changes made by Schenderling are assessed and improvements are suggested. Section 4.3 looks into the possibility of implementing a correlation for the Nusselt number that better describes supercritical flow.

4.1 Spoelstra Heat Transfer Model

In the first version of the code, made by Spoelsta, the heat flux was uniformly distributed across each core section according to the simple equation (4.1). Spoelsta chose to assume the heat flux would roughly be the same as the production, making the heat flux constant over each core segment. The losses to the environment are modeled as a fixed percentage of production. This simplified the heat transfer significantly.

$$q'_{core} = \frac{P_{core}(1 - p_{loss})}{L_{core}} \tag{4.1}$$

In this equation q'_{core} is the linear heating rate in W/m, with P_{core} being the power supplied to the core segment and L_{core} the length of the core segment. p_{loss} is the percentage of the power lost to the envoirment. However, there are two considerable problems with this simplification. First, this assumption made in the Spoelstra model does not hold when the heat transfer coefficient varies. A higher heat transfer coefficient means a lower relative temperature difference is necessary to reach the same heat flux and vice versa, see equation (4.2).

$$q''_{core} = \alpha \Delta T \tag{4.2}$$

With ΔT being the relative temperature between the facility wall and the fluid bulk and α the heat transfer coefficient. In the operating window of the SCWR the properties of Freon change drastically, which strongly influences the heat transfer coefficient. Thus for the heat flux to remain constant ΔT must change significantly as well. However, the losses to the environment also depend on the relative temperature, i.e. the relative temperature between the DeLight wall and the environment. Spoelsta assumed these losses to be constant as well, i.e. a fixed percentage of core power. The simplification made by Spoelstra lead to an inaccurate description of heat transfer when the heat transfer coefficient in the system is

variable. Literature suggest this is the case in a SCWR(Piore et al., 2011). The Spoelstra model does not accurately describe the complex heat transfer dynamics of the DeLight facility.

The second problem is the absence of thermal inertia. Density wave oscillations play a major role in the stability analysis. The energy stored in the walls of the core are expected to have a damping effect on DWO's. The relative temperature between the wall and bulk fluid will likely be lower for hotter areas compared to the colder areas. This will result in a slightly lower heat flux for hotter areas while cooler areas experience a higher heat flux, see equation (4.2). However, it is also possible that a hotter area will have a higher heat flux due to the heat transfer coefficient growing due to a dependency on temperature. Then the DWO will grow larger in amplitude. This complex behavior will be further investigated in this thesis.

4.2 Schenderling's Implementation

To better represent the heat transfer in the DeLight facility, Schenderling(2013) altered the Spoelstra model to include a more complex heat transfer model and thermal inertia in the walls. For this adjusted heat transfer model the wall temperature must be calculated since the temperature difference between facility wall and bulk fluid has to be know. Schenderling made an analysis of the energy balance in the core and proposed the following equation (4.3).

$$\rho_{wall} C_{p,wall} V_{wall} \frac{dT_{wall}}{dt} = Q - \alpha_{in}(T_{wall} - T_{freon}) Per_{in} dz - \alpha_{out}(T_{wall} - T_{ambient}) Per_{out} dz \quad (4.3)$$

The term on the left hand side is the temporal change of energy contend in the facility wall, which is the result of the energy production Q minus the energy transferred to the fluid bulk and the energy loss to the environment. In the new model both the heat flux to the fluid bulk and the environment become functions of the stream-wise position in the core section. This is a much more complex representation than the one of Spoelstra. Note that friction heat is still ignored and axial heat conduction is not considered. Equations (4.4) and (4.5) show the relation of the heat flux to the fluid bulk and the environment.

$$Q'_{in}(z) = \alpha_{in}(z)(T_{wall}(z) - T_{freon}(z)) Per_{in} \quad (4.4)$$

$$Q'_{out}(z) = \alpha_{out}(z)(T_{wall}(z) - T_{ambient}) Per_{out} \quad (4.5)$$

4.2.1 External Heat Flux

The external heat flux is almost entirely dictated by the temperature difference between the core pipe segments and the environment. Because the temperature of the environment can be seen as constant the heat flux is nearly constant as well, see equation (4.8). Equation (4.6) is an approximation of the heat transfer coefficient.

$$\alpha_{out}(z) = Nu_{out}(z) \frac{\lambda_{air}}{D} \quad (4.6)$$

With Nu_{out} as the Nusselt number for natural converction outside the verticatical cilinderis, proposed by Le Fevre and Ede(1956) and Gr as the Grashof number.

$$Nu_{out}(z) = \frac{4}{3}\left(\frac{7GrPr_{out}^2}{5(20+21Pr_{out})}\right)^{\frac{1}{4}} + \frac{4(272+315Pr_{out})L}{35(64+63Pr_{out})D} \tag{4.7}$$

$$Gr = \frac{g\beta(T_{wall}-T_{ambient})D^3}{\nu^2} \tag{4.8}$$

Schenderling assumed the volumetric thermal expansion coefficient β can be written as $(1/T_{avg})$, which is only correct for ideal gasses. Furthermore, the average values are used to calculate the Grashof number. This was done because of the effect of the grashoff number is small and precise calculation is fairly tedious. The calculation of the Grashoff number was not changed in this thesis.

4.2.2 Internal Heat Flux

The dependency of the internal heat flux(equation (4.4)) on ΔT and the perimeter of the core pipes is straightforward and very similar the the external heat flux. The heat transfer coefficient on the other hand is more complex and considerable simplifications ware made by Schenderling. Equation (4.9) is an approximation of the heat transfer coefficient.

$$\alpha_{in}(z) = Nu_{in}(z)\frac{\lambda_{freon}}{D_H} \tag{4.9}$$

In the model the thermal conductivity λ is not a known variable so Schenderling estimated this to be constant. However this is not the case, it varies like the density and viscosity do due to the supercritical conditions. Furthermore, in most of schenderling's calculations the Nusselt number was calculated with the Dittus-Boelter(1930) equation for forced convection in turbulent pipes, equation (4.10).

$$Nu_{in}(z) = 0.027Re_z^{0.8}Pr_{in}^{0.3333} \tag{4.10}$$

Usually, this correlation is fairly accurate for subcritical flow. However, to further simplify the model, Schenderling chose to assume the Prandtl number constant. For supercritical flow near the pseudo-critical point this is not at all the case. The Prandtl number strongly depends on the thermal conductivity, viscosity and heat capacity. All these properties change significantly in the pseudo-critical region. But even if the Prandtl number would have been properly calculated, Dittus-Boelter does not account for pseudo-film boiling. When pseudo-film boiling takes place a thin layer of fluid is heated to a value near or higher than the pseudo-critical point. This layer expands, as the density decreases, and causes the fluid layer to accelerate. This results in a lower friction factor, see chapter 3, causing the bulk to more easily move trough the core, extinguishing turbulence. Turbulence increases heat transfer and thus pseudo-film boiling causes deteriorated heat transfer. Once the fluid bulk is approaching pseudo-critical temperatures, however, the fluid bulk will also stat to expand, greatly increasing turbulence and hence heat transfer.

4.3 Choice of New Nusselt Correlation

To better approximate the behavior of the heat transfer in the DeLight facility the thermal conductivity and Prandtl number will be modeled more realistically. Also a new correlation to calculate the Nusselt number, one that better captures the supercritical behavior, will be implemented. Similarly to the friction factor model, many correlations have been proposed. Unfortunately they do not agree well with respect to each other. Recently, Zahlan et al.(2010) made an analysis of the most widely used supercritical Nusselt correlations. The result of this effort is shown in table 4.1.

Table 4.1: Weighted average and RMS errors in each of the supercritical sub-regions. (Source: Zahlan et al., 2010)

Correlation*	Supercritical Region				Region	
	Liquid-Like		Gas-Like		Critical or Pseudocritical	
	Errors, %					
	Average	RMS	Average	RMS	Average	RMS
Bishop et al. (1965)	6.3	24.2	5.2	18.4	20.9	28.9
Swenson et al. (1965)	1.5	25.2	-15.9	20.4	5.1	23.0
Krasnoshchekov et al. (1967)	15.2	33.7	-33.6	35.8	25.2	61.6
Watts & Chou (1982)	4.0	25.0	-9.7	20.8	5.5	24.0
Chou (1982)	5.5	23.1	5.7	22.2	16.5	28.4
Griem (1996)	1.7	23.2	4.1	22.8	2.7	31.1
Jackson (2002)	13.5	30.1	11.5	28.7	22.0	40.6
Mokry et al. (2009)	-3.9	**21.3**	-8.5	**16.5**	**-2.3**	**17.0**
Kuang et al. (2008)	-6.6	23.7	**2.9**	19.2	-9.0	24.1
Cheng et al. (2009)	**1.3**	25.6	**2.9**	28.8	14.9	90.6
Hadaller & Benerjee (1969)	7.6	30.5	10.7	20.5	-	-
Sieder & Tate (1936)	20.8	37.3	93.2	133.6	-	-
Dittus & Boelter (1930)	32.5	46.7	87.7	131.0	-	-
Gnielinski (1976)	42.5	57.6	106.3	153.3	-	-

In bold – the minimum values.
* many of these correlations can be found in Pioro and Duffey (2007).

Schenderling briefly studied the effect of changing the Nusselt correlation in the model to a supercritical correlation, namely the ones proposed by Jackson and Bishop, and found the new correlation having an effect on the neutral stability boundary. However, no definitive conclusion could be reached, with respect to the effect on the stability. To further investigate the behavior of the Nusselt number in supercritical state, three models where chosen based on the results by Zahlan et al.(table 4.1) and the possibility of implementation in the model. The chosen models are the ones by Bishop, Jackson and Mokry.

4.3.1 Bishop et al. (1965)

Bishop conducted experiments in 1964 using supercritical water to find the following correlation (4.11). The supercritical water used flowed upwards inside vertical bare tubes. The last term of the expression accounts for the entrance effect. The measurements used for the

correlation are performed in the same range as the SCWR operating range.

$$Nu_B = 0.0069 Re^{0.9} \bar{Pr}^{0.66} \left(\frac{\rho_w}{\rho_b}\right)^{0.43} \left(1 + 2.4\frac{D}{x}\right) \tag{4.11}$$

4.3.2 Jackson (2002)

Jackson's correlation (4.12) is a modification of the original Krasnoshchekov et al.(1967) correlation to employ the Dittus-Boelter form if the relative temperature is zero. This correlation is based on measurements from supercritical water and carbon dioxide, forced convection heat transfer.

$$\begin{aligned}
Nu_J &= 0.0183 Re^{0.82} Pr^{0.5} \left(\frac{\rho_w}{\rho_b}\right)^{0.3} \left(\frac{\bar{C}_p}{C_{p,b}}\right)^n && (4.12)\\
n &= 0.4 \; T_b < T_w < T_{pc} \; and \; 1.2T_{pc} < T_b < T_w && (4.13)\\
n &= 0.4 + 0.2\left(\frac{T_w}{T_{pc}} - 1\right) \; T_b < T_{pc} < T_w && (4.14)\\
n &= 0.4 + 0.2\left(\frac{T_w}{T_{pc}} - 1\right)\left[1 - 5\left(\frac{T_w}{T_{pc}} - 1\right)\right] \; T_{pc} < T_b < 1.2T_{pc} \; and \; T_b < T_w && (4.15)
\end{aligned}$$

4.3.3 Mokry et al. (2009)

The most recent correlation (4.16) that will be assessed is Mokry et al. This correlation is based on a new set of heat-transfer measurements and the latest properties of water(NIST, 2007). The measurements where done within the SCWR range of operation and the experimental data agreed with the correlation with a spread of roughly 25% of the calculated heat transfer coefficients.

$$Nu_M = 0.0061 Re_b^{0.904} \bar{Pr}_b^{0.684} \left(\frac{\rho_w}{\rho_b}\right)^{0.564} \tag{4.16}$$

Chapter 5

Experimental Procedure

Chapter 5 gives an overview of the numerical model and the experimental procedures. First, some aspects of the model are explained in section 5.1 after which some adjustments are proposed in section 5.2. Section 5.3 discusses a behavior analysis of the selected supercritical models. The experimental procedure for steady-state and stability analysis are the subject of respectably section 5.4 and 5.5.

5.1 Numerical Model

A short description of the DeLight model will be given in this section. For a full explanation of the model, please see Spoelstra(2012). A combination of the forward and backwards Euler Scheme is used to discretize the model equations derived by Spoelstra. The forward Euler scheme is explicit, accurate and computationally cheap. However, to ensure numerical stability, sufficiently small steps need to be taken which in turn is computationally demanding. The backwards Euler scheme is implicit. This scheme is unconditionally stable but computationally demanding and less accurate. A scheme that combines an implicit and an explicit scheme is called semi-implicit. The semi-implicit scheme in the DeLight model combines the forward and backwards Euler scheme. θ is a system input-variable that dictates which scheme is dominant in the calculation of the system differential equations. $\theta = 1$ is fully implicit and $\theta = 0$ fully explicit.

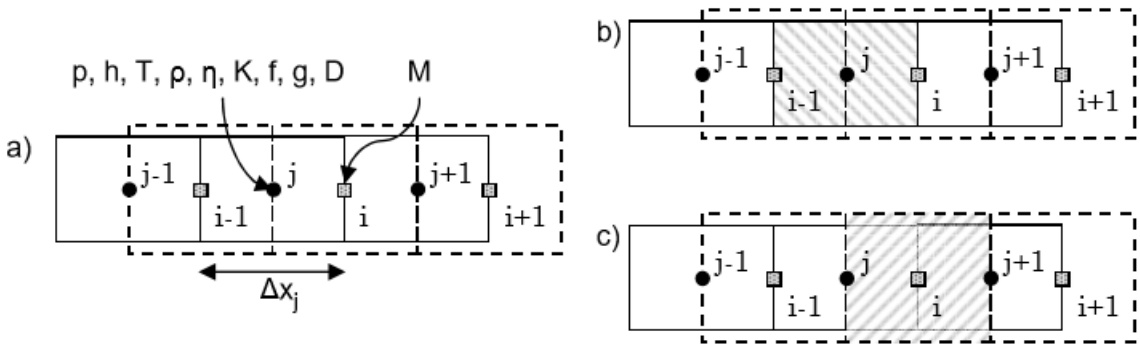

Figure 5.1: Schematic representation of control volumes and staggered grid in the DeLight model(a) volume around the point over which the mass en energy balance are integrated(b) volume around the point over which the momentum balance is integrated(c). (Source: Spoelstra, 2012)

To prevent odd-even decoupling of the pressure field, the systems differential equations are discretized on a staggered grid(see figure 5.1a). The momentum balance is solved at position i while the energy and mass balance are solved at position j. Consequentially the energy and mass balance are integrated over the area around j (see figure 5.1b) and the momentum balance is integrated over the area around i (see figure 5.1c).

Figure 5.3 is a flowchart of the numerical DeLight model. Here the two loops can be seen; the red box is the pressure correction loop and the blue box the time stepping loop. Each time step starts by defining the heat flux withing the system, after which the pressure correction loop is initiated. This loop starts by solving the enthalpy balance using the newly defined heat flux and variables from previous iterations. The enthalpy balance yields the new bulk enthalpy which defines bulk properties as the thermal conductivity, density, temperature, viscosity and heat capacity. With these bulk variables and the mass-flow from the previous iteration, the Darcy-Weisbach friction factor is calculated. The next step is solving the momentum balance and several correction functions to determine the mass-flow while correcting the system pressure. This mechanism is described by Spoelstra(Spoelstra, 2012) and will not be discuses further in this thesis. After these steps, there is a check to see if the required convergence is reached. If no, the loop will be reiterated. If yes, the second part of the time-step loop is initiated and the wall temperature will be determined using the discretized form of equation (4.3). Finally, several variable are stored and the next time step is initiated.

5.2 Model Adjustment

The DeLight model does not accurately predict the stability of the DeLight facility. In chapter 3 and 4, several improvements have been proposed. First of all a new third order spline will be added for the thermal conductivity. The spline is built with Matlab and based on NIST data from 2013(see figure 5.2). The choice of a spline is in line with Spoelstra and keeps the computational demand low. The process, "call splines"(see figure 5.3), in the pressure correction loop now includes this spline. Also, the heat capacity is now calculated here.

In the Schenderling model the wall temperature is known but the properties near the wall such as enthalpy, density, viscosity and heat capacity are not calculated. These wall properties are necessary to implement the supercritical models discussed in chapter 3 and 4. To obtain these properties in the model a new step is added, "call wallsplines"(see figure 5.3). Each time the wall temperature in a times step has been determines the wall enthalpy, density, viscosity and thermal conductivity will be calculated using splines. The splines used are the same as the splines used for the bulk properties, except for the temperature being the input instead of the enthalpy. With the more accurate description of the thermal conductivity and the calculation of the heat conductivity the definition of the Prandtl number can now be implemented, which is necessary for a proper calculation of the Nusselt number.

Combining the effects of these changes, a new friction factor and Nusselt number correlation are implemented. The friction factor and wall temperature calculation now require wall properties(see figure 5.3).

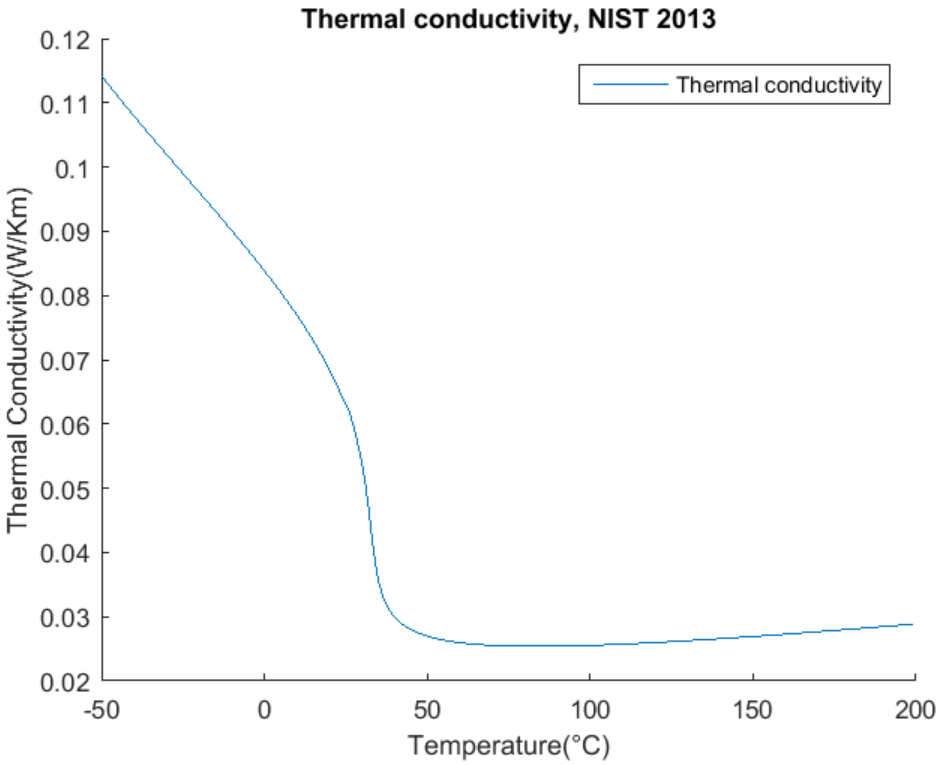

Figure 5.2: Thermal conductivity of R23 around the pseudo-critical point, 33.22 °C at 57 bar. Plotted with NIST data, 2013.

5.3 Supercritical Behavior Study

Because supercritical behavior is complex and several heating/cooling effects take place at the same time, like pseudo-film boiling, a computational analysis of the behavior of the friction factor and the Nusselt number is done. Within the DeLight model it is difficult to see and predict the behavior of the supercritical models, which is why the analysis is done separately, in a time-independent scenario. The models chosen in chapter 3 and 4 were assessed in a situation with a constant temperature difference between the wall and the bulk. The mass-flow was held constant while the bulk temperature was slowly increased at exactly the same rate as the increase in the wall temperature, thus keeping the temperature difference constant at either 0, 15, 30 or -30 degrees. Physically this would be nearly impossible to achieve, however, it can disclose some valuable information while comparing the different models. Both the friction factor models, Nusselt correlations and heat transfer coefficients are compared using this method.

5.4 Steady-State

The analysis of the DeLight model can be divided in two parts; steady-state and stability analysis. Steady-state is reached by gradually increasing core power to the set level while solving the system equations of state. During the simulations a time of 2000 seconds was chosen to increase the core power, followed by 500 seconds to settle into a steady-state situation. This procedure is equivalent to Spoelstra's method. During the acquisition of steady-state $\theta = 1$, so only the backwards Euler scheme is used, making the time-stepping fully implicit.

In steady-state the changes to the friction factor, thermal conductivity, Prandtl number, Nusselt number, heat transfer coefficient and heat flux will be analyzed. The magnitude and type of changes can help explain a possible shift of the neutral stability boundary. Also, the steady-state mass-flow will be determined and compared to the experimental values and the power flow maps made by Spoelstra. A power flow map is a plot where steady-state mass-flow is plotted against the core power at a certain core inlet temperature.

5.5 Stability

The second part will be the stability analysis, during which it is determined whether a perturbation grows or decreases over time, i.e. indicated by the decay ratio. The steady-state simulation is used as the initial condition for the stability calculation. Stability analysis requires smaller time-steps to accurately model the oscillations, especially if the frequency of the oscillation is high. To achieve a significant accuracy a much smaller time step is chosen, $0.01s$ instead of $1s$. Additionally, θ is set to 0.6. This increases numerical precision making use of the semi-implicit scheme. Spoelstra tested several methods to create a perturbation however it turned out that the switching to the finer grid created enough of a disturbance(order of 1%). To determine the stability of the system the autocorrelation of the time signal is analyzed. Similarly to the DeLight measurements, a function is fitted to the autocorrelation function, disclosing the frequency and corresponding decay ratio. Spoelstra extended the fitting function used in the DeLight measurements (2.1) with extra terms for resonance containing multiple frequencies. In case of three frequencies the fitting function takes from as seen in equation (5.1). The corresponding decay ratio and frequency are then yielded respectively by equation (5.2) and (5.3).

$$y = a_0 + \left(1 - a_0 - \sum_{i=2}^{4} a_i\right) e^{b_i \tau} + \sum_{i=2}^{4} a_i e^{b_i \tau} cos(\omega_i \tau) \tag{5.1}$$

$$DR_i = e^{\frac{2\pi b_i}{|\omega_i|}} \tag{5.2}$$

$$f_i = \frac{|\omega_i|}{2\pi} \tag{5.3}$$

The stable versus unstable points are plotted in a dimensionless plane spanned by N_{PCH} and N_{SUB}. The definitions of these dimensionless numbers are given by equations (5.4) and (5.5). Each combination of these dimensionless number represent a working point for the model and the DeLight facility. All working points represent a combination of core power, core inlet temperature and steady-state mass-flow.

$$N_{SUB} = \frac{h_{pc} - h_{in}}{h_{pc}} \tag{5.4}$$

$$N_{PCH} = \frac{P_{core}}{M h_{pc}} \tag{5.5}$$

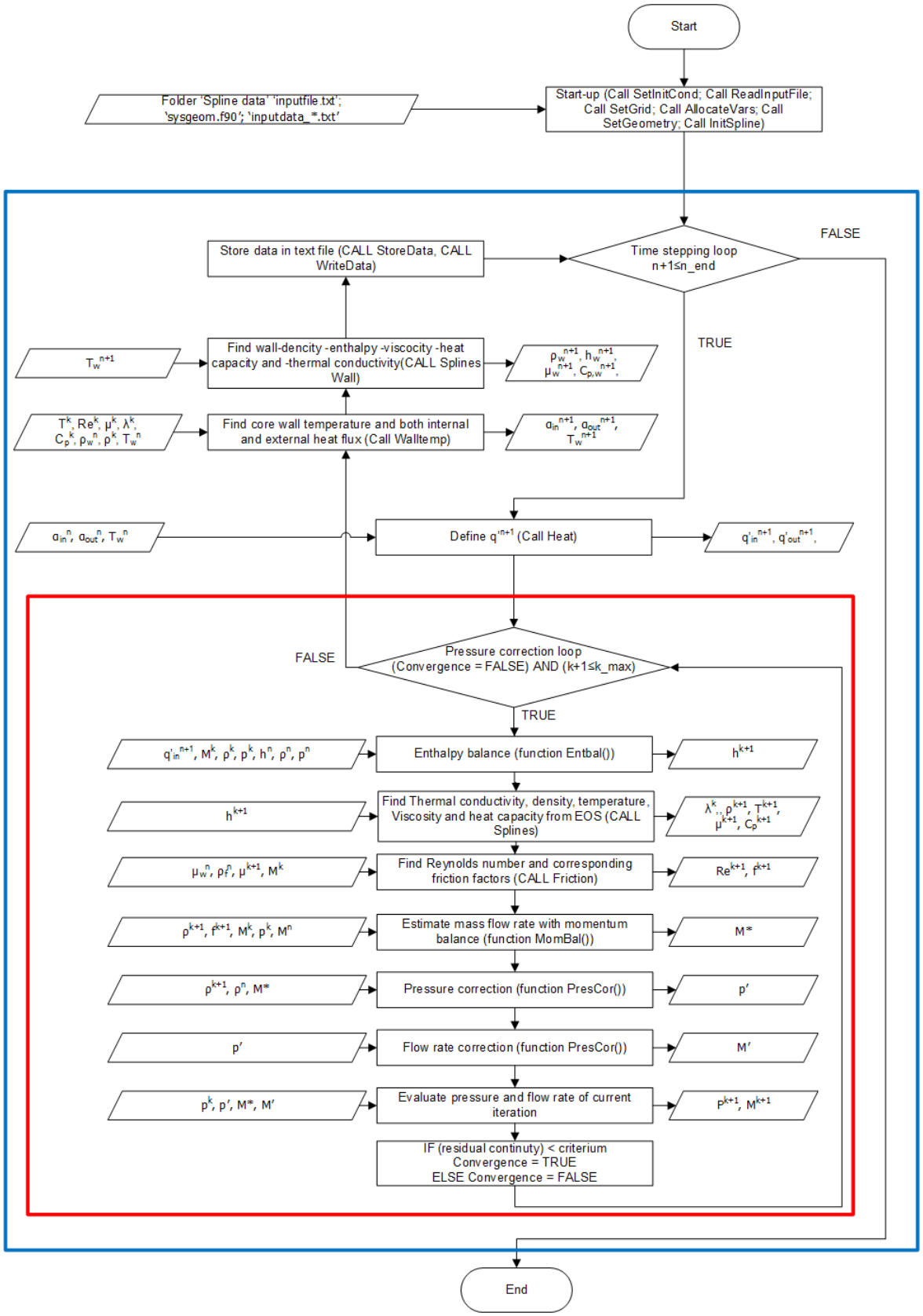

Figure 5.3: Flowchart of the numerical model. The start-up phase is simplified into a single process. The blue box indicates the time stepping g loop and the red box the pressure correction iteration.

Chapter 6

Supercritical Behavior Analysis

This chapter assesses the behavior predicted by several Nusselt number and friction factor correlations during supercritical heating/cooling. Section 6.1 discusses the friction factor and section 6.2 the Nusselt number and heat transfer coefficient. Section 6.3 discusses the current implementation of the Dittus-Boelter correlation in the Schenderling model.

6.1 Friction Factor

The first comparison that is made between the different friction factor models, is a situation where there is no difference between the wall and bulk temperature. This yields isothermal friction factors, i.e. the supercritical terms do not manifest themselves as $\mu_w = \mu_b$ and $\rho_w = \rho_b$. The result of this simulation is figure 6.1.

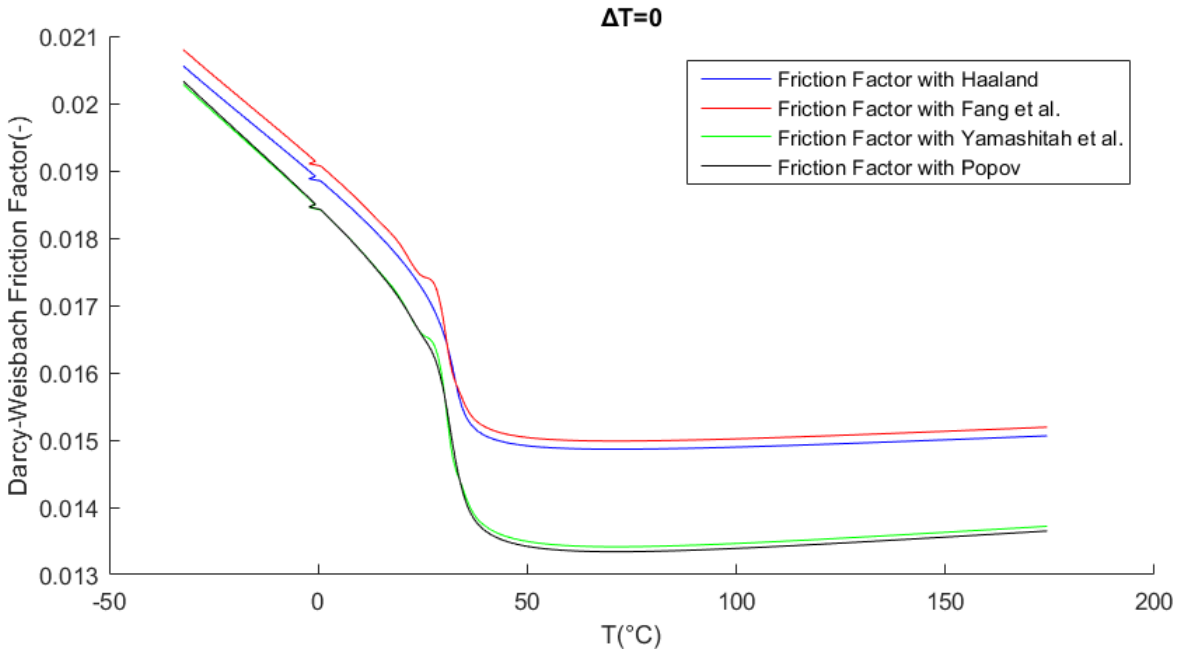

Figure 6.1: Behavior of the friction factor according to several correlations at ΔT=0 °C. On the horizontal axis the temperature of the bulk is displayed, this means the wall temperature at that point is $T_{bulk} + \Delta T$. The Darcy-Weisbach friction factor is displayed on the vertical axis.

The isothermal friction factors portray the expected behavior as the density and viscosity

drop near the pseudo-critical point. Of course, the drop in density causes v to increase as the mass-flow is constant during the calculation. The friction factor thus decreases as the Reynolds number grows larger, see equation (6.1).

$$Re = \frac{\rho v L}{\mu} = \frac{M D_{tube}}{\mu A} \tag{6.1}$$

The Fang correlation almost perfectly agrees with Haaland while in the gas-like region the Yamashitah and Popov correlation predict a different friction factor. In the second simulation ΔT=30 °C and maintained as the bulk temperature increases (see figure 6.2). In this simulation the supercritical terms play a significant role as a large drop of the friction factor around the pseudo-critical point is predicted. The Fang and Yamashitah correlations experience a low point roughly 20 °C before the pseudo-critical point. This makes sense, as the difference between the bulk and wall properties reaches its maximum in this area. After the pseudo-critical point, the difference in properties becomes smaller and the friction factor approaches the isothermal friction factor again. The Popov correlation however does not predict such a large gap. This is due to the fact Popov uses the ρ_f in stead of ρ_w. Despite this disagreement, it is clear the friction factor decreases significantly during supercritical heating.

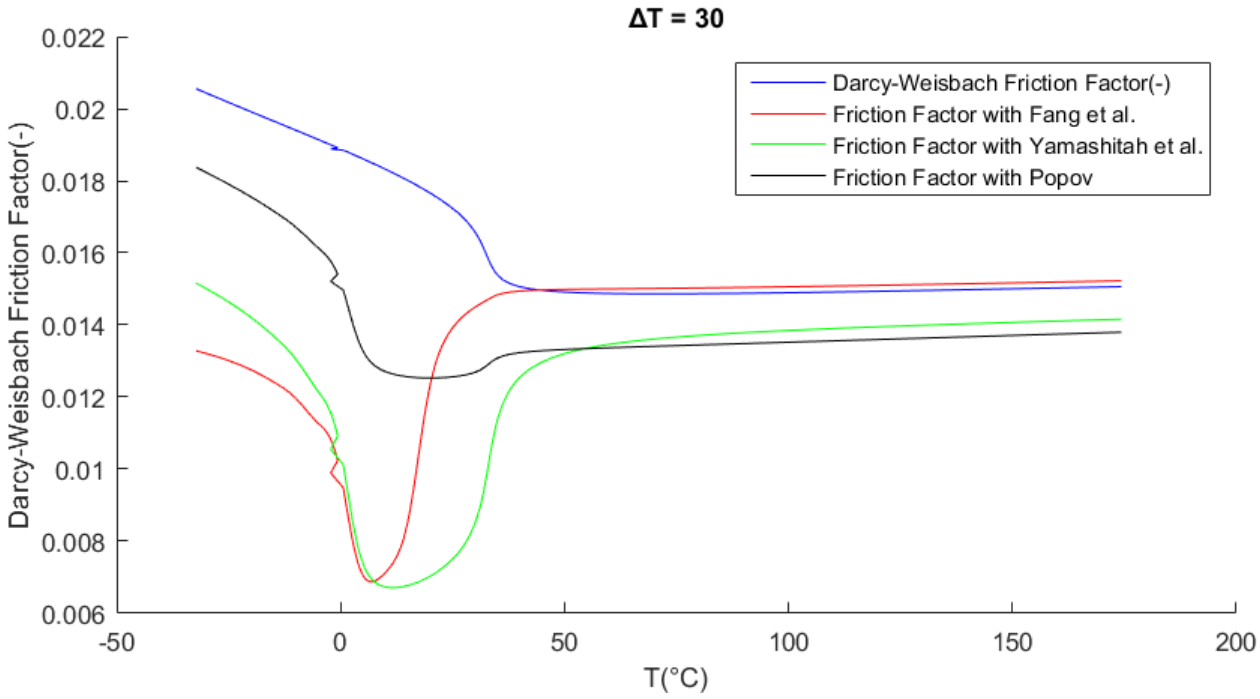

Figure 6.2: Behavior of the friction factor according to several correlations at ΔT=30 °C. On the horizontal axis the temperature of the bulk is displayed, this means the wall temperature at that point is $T_{bulk} + \Delta T$. The Darcy-Weisbach friction factor is displayed on the vertical axis.

The behavior of the friction factor during supercritical cooling has also been assessed (see figure 6.3). The effects are the opposite of the ΔT=30 °C case. This finding agrees with the available literature. The order of the deviation also appears to be equivalent to the supercritical heating. As the fluid cools near the wall the density and viscosity increase and because the mass-flow remains constant the Reynolds number decreases thus the friction factor spikes. The peak however, shifted to roughly 20 °C after the pseudo-critical point. Again,

as the difference in properties become smaller the isothermal friction factor is approached.

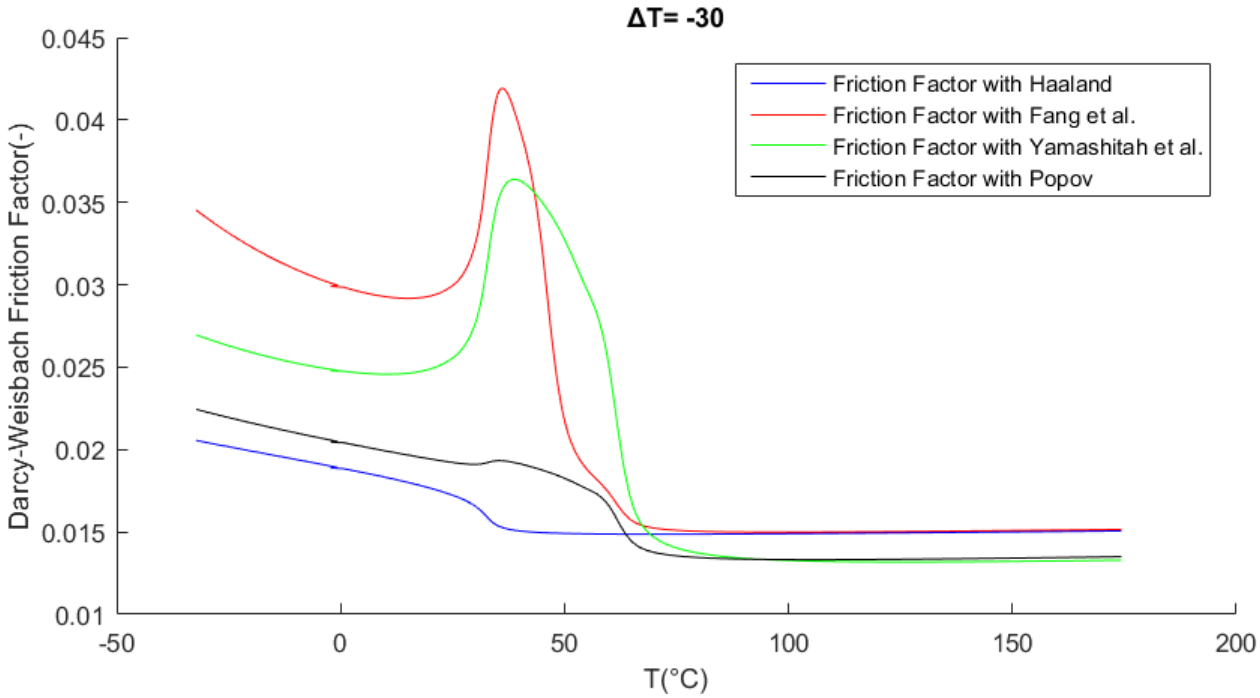

Figure 6.3: Behavior of the friction factor according to several correlations at ΔT=$-$30 °C. On the horizontal axis the temperature of the bulk is displayed, this means the wall temperature at that point is $T_{bulk} + \Delta T$. The Darcy-Weisbach friction factor is displayed on the vertical axis.

From the work done by Schenderling, it can be concluded a a relative temperate of 30 °C between core wall and bulk within the DeLight core is not a fictional case. Thus, it is clear Haaland cannot accurately capture the friction factor in the DeLight core. Given the results of this chapter, the correlation proposed by Fang et al. has been chosen for implementation in the DeLight model. There are three reasons why this correlation has been chosen over the others. First, it has shown to give the lowest relative error in the study done by Fang et al.(2012), see table 3.1. Second, the isothemal term of the Fang correlation agrees with Haaland outside the core. Considering that Spoelstra, with the Haaland correlation, was able to approach the experimental steady-state mass-flow quite nicely, this is seen as an advantage. Lastly, the height of the friction factor at the peak/gap agrees relatively well with Yamashitah et al., giving the its prediction some legitimacy. Still, it should be noted all correlations have relatively large errors and none of the assessed correlations are based on R23.

6.2 Heat Transfer Model

The first case is a calculation of the Nusselt number and the heat transfer coefficient with ΔT=0 °C. The result can be found in figure 6.4. The only difference between the heat transfer coefficient and Nusselt number is the term $\lambda_{Freon,b}/D_H$ from equation (4.9). As the thermal conductivity decreases with increasing temperature(see figure 5.2) this term becomes smaller, lowering the right branch in the heat transfer coefficient plot. The behavior of the different models is fairly similar; all correlations show a peak at the pseudo-critical point and outside the pseudo-critical region they more or less agree with each other. The height of the peak

can be explained by the extend of the power applied to the Prandtl number, i.e. Bishop and Mokry apply a power of respectably 0.684 and 0.66 versus Jackson's 0.5 and Dittus-Boelter's 0.4. A higher power results in a higher peak. The second simulation is the ΔT=30 °C case, see figure 6.6. The effect of pseudo-film boiling is a evident, as the heat transfer significant deteriorates in the Bishop and Mokry model. The heat transfer coefficient still experiences a peak around the pseudo-critical point but it is much lower than the ΔT=0 °C case. Note that Jackson's correlation includes some discontinuities, these discontinuities represent a position where the expression for n changes. As expected, the heat transfer coefficient calculated with Dittus-Boelter is obviously not effected by a heated wall.

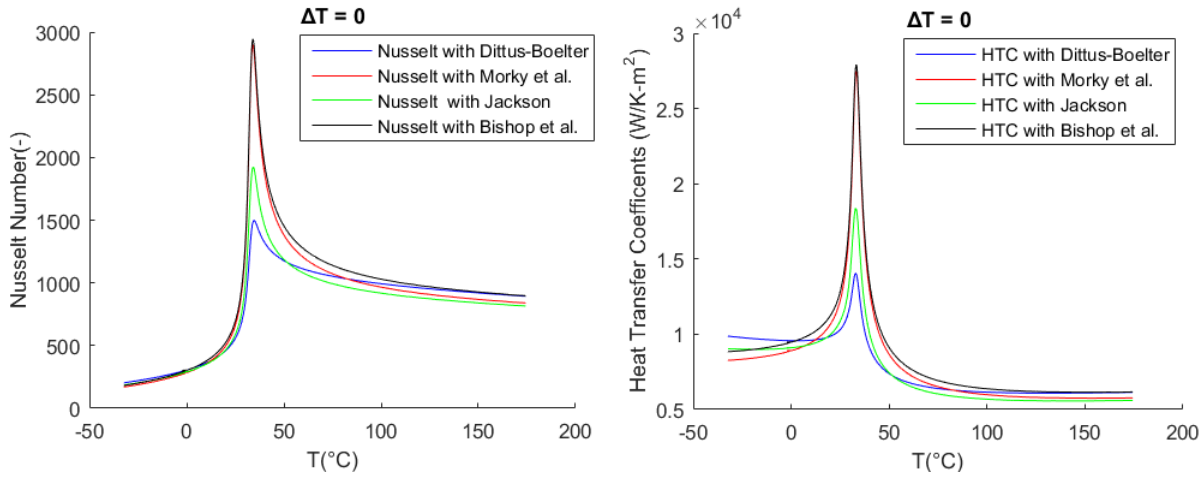

Figure 6.4: Plot of the heat transfer coefficient(left) and Nusselt number(right), according to several correlations at ΔT=0 °C. On the horizontal axis the temperature of the bulk is displayed, this means the wall temperature at that point is $T_{bulk} + \Delta T$. The heat transfer coefficient and Nusselt number are displayed on the vertical axis.

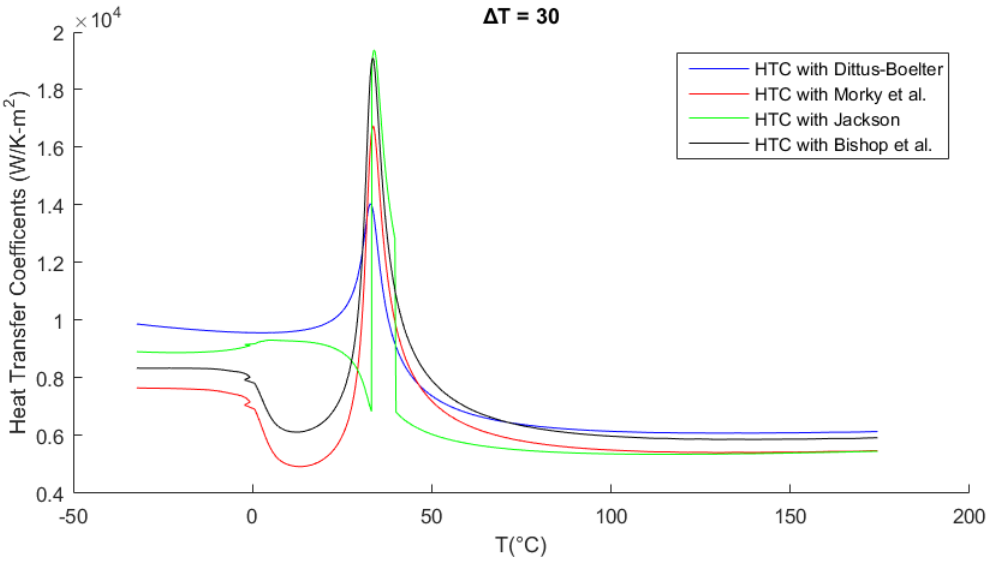

Figure 6.5: Plot of the heat transfer coefficient according to several Nusselt correlations at ΔT=30 °C. On the horizontal axis the temperature of the bulk is displayed, this means the wall temperature at that point is $T_{bulk} + \Delta T$. The heat transfer coefficient is displayed on the vertical axis.

After the supercritical heating simulation, a supercritical cooling case was assessed, with $\Delta T = -30$. The effect of pseudo-film boiling now has the opposite effect, i.e. a dense layer of fluid forms near the wall. This dense layer enables the bulk of the fluid to transfer more energy thus increase heat transfer. Again, the Bishop and Mokry correlation show the same type of behavior while Dittus-Boelter does not change. Jackson's correlation does not feature discontinuities in this case because the value of n is unchanged as $T_{bulk} > T_{wall}$, see equation (4.12).

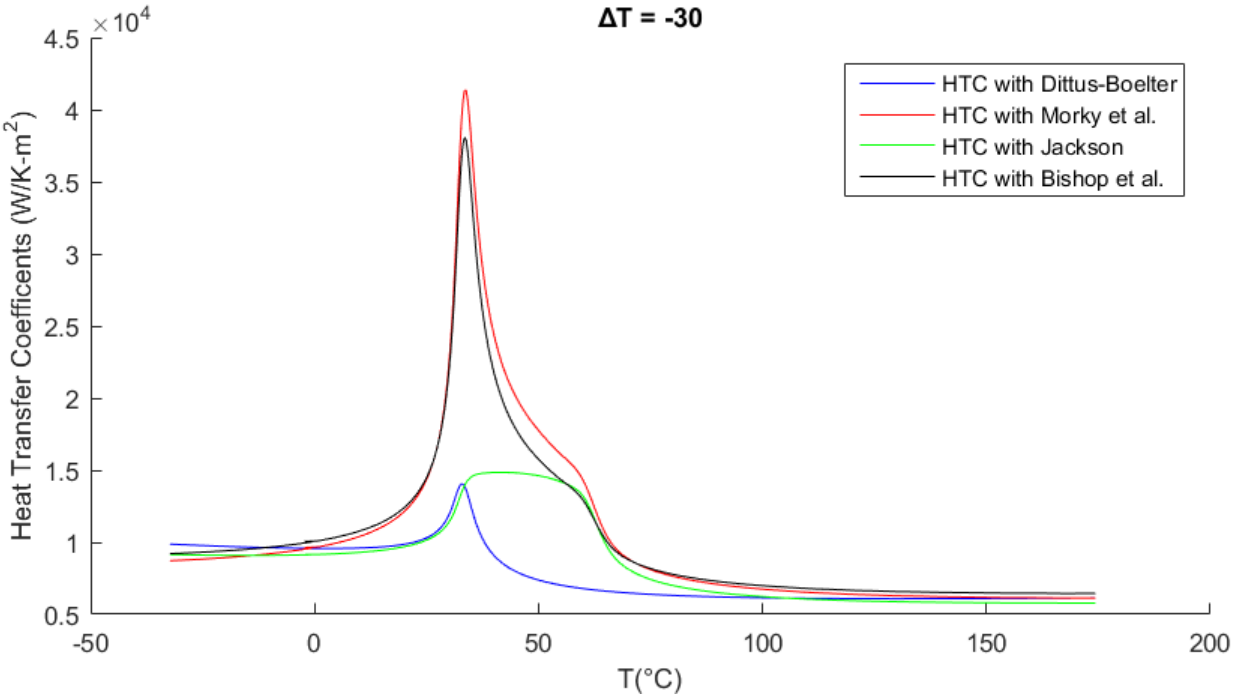

Figure 6.6: Plot of the heat transfer coefficient according to several Nusselt correlations at ΔT=$-30\,^{\circ}$C. On the horizontal axis the temperature of the bulk is displayed, this means the wall temperature at that point is $T_{bulk} + \Delta T$. The heat transfer coefficient is displayed on the vertical axis.

Overall, the deviation of the supercritical Nusselt correlations versus the Dittus-Boelter correlation is significant. The behavior the supercritical correlations portray, is more complex and very sensitive to the temperature difference between the bulk and wall fluid. Therefore, it is clear Dittus-Boelter cannot accurately capture the behavior of the Nusselt number during supercritical heating/cooling, especially in the pseudo-critical region. To improve the heat transfer model, the Mokry correlation will be implemented in the DeLight model. Mokry's correlation performed well in the study done by Zahlan et al.(2010) Also, the measurements to derive the correlation were done in the operating window of the SCWR with the latest data from NIST. Lastly, Bishop found the same general behavior as Mokry legitimizing the findings.

6.3 Schenderling Implementation of the Dittus-Boelter Correlation

Chapter 4 discussed some of the assumptions made by Schenderling(2013). To get a better understanding of how those assumptions effected the heat transfer coefficient and the Nusselt

number, a final calculation was conducted(see figure 6.7). In this simulation, the Dittus-Boelter correlation is plotted against the current implementation of Dittus-Boelter in the model, i.e. with $\lambda = 0.0414$ W/K*m and $Pr = 6$. It is clear that the assumptions completely change the heat transfer behavior, especially in superheater I and superheater II. Here, the heat transfer coefficient is a factor 2.5 higher than the model actually predicts.

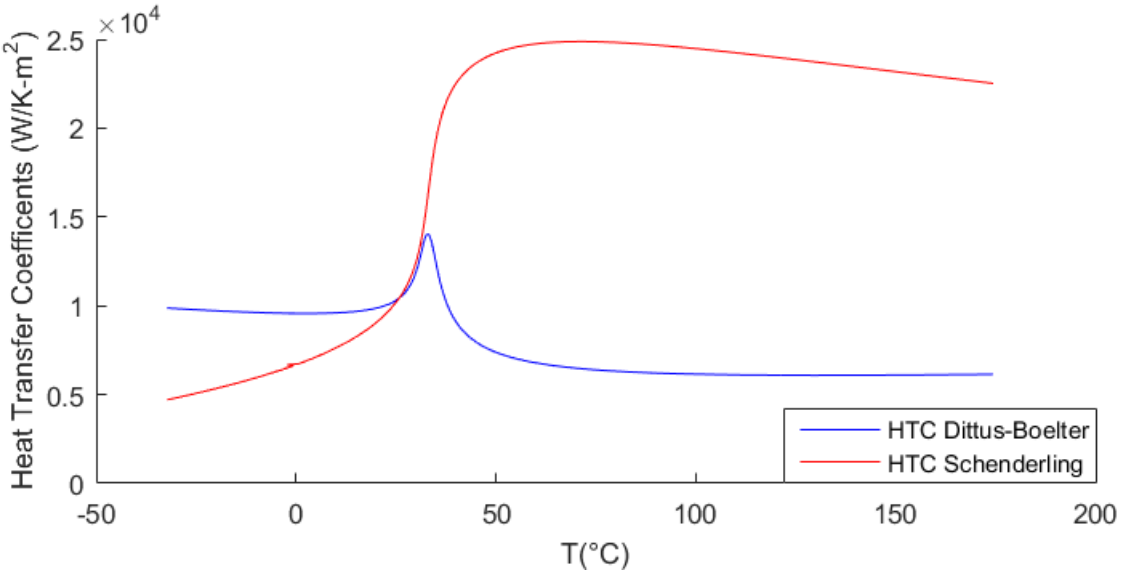

Figure 6.7: Plot of the heat transfer coefficient according to the Dittus-Boelter correlation versus the Schenderling implementation in the model. On the horizontal axis the temperature of the bulk is displayed. The heat transfer coefficient is displayed on the vertical axis.

Chapter 7

DeLight Model Results

7.1 Steady-State

7.1.1 Friction Model

The first change to the DeLight model is the friction factor model proposed by Fang et al. The implementation is quite straightforward. The steady-state result is captured in figure 7.1. As expected Fang's friction factor strongly decreases in the core segments while Haaland and the isothermal term in Fang's correlations only decrease because of an increasing Reynolds number. Because $\Delta T = 0\,^{\circ}C$ outside of the core, the friction factors agree well outside the core. It was decided not to implement the new model in the heat exchanger, as the friction factor there is experimentally determined by Spoelstra and the heat exchangers are simplified in the model.

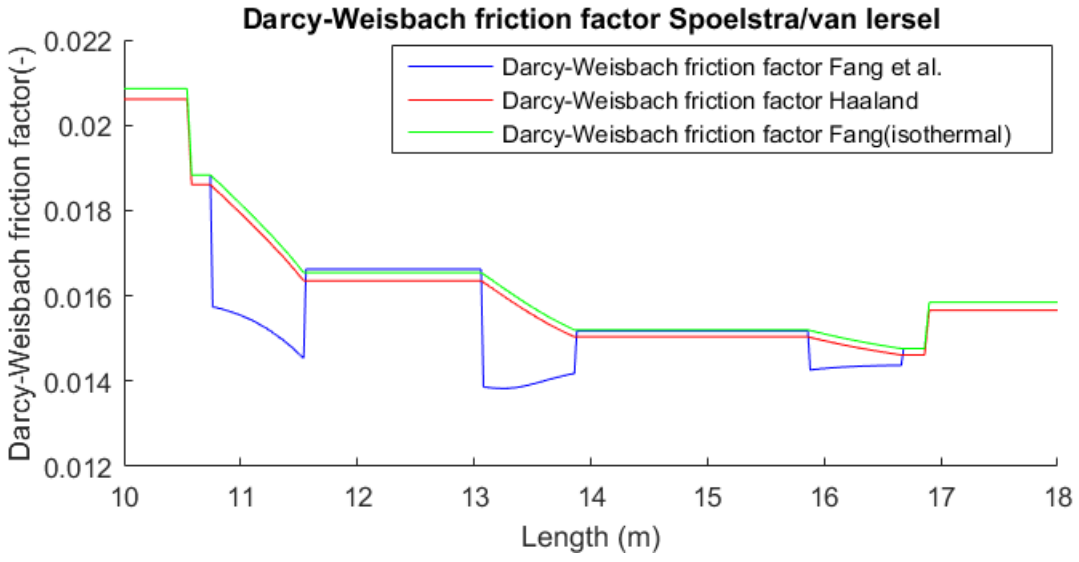

Figure 7.1: Friction factor in the DeLight core. On the vertical axis the friction factor is displayed and the horizontal axis represents the location in the model. The three core segments are clearly distinguishable because of the smaller friction factor

7.1.2 Heat Transfer Model

A 3^{rd} order spline for the thermal conductivity was added to the model and, consequently, a more realistic value for the bulk Prandtl number was calculated (see figure 7.2 and figure 7.3). A more detailed description of the spline, can be found in appendix B.

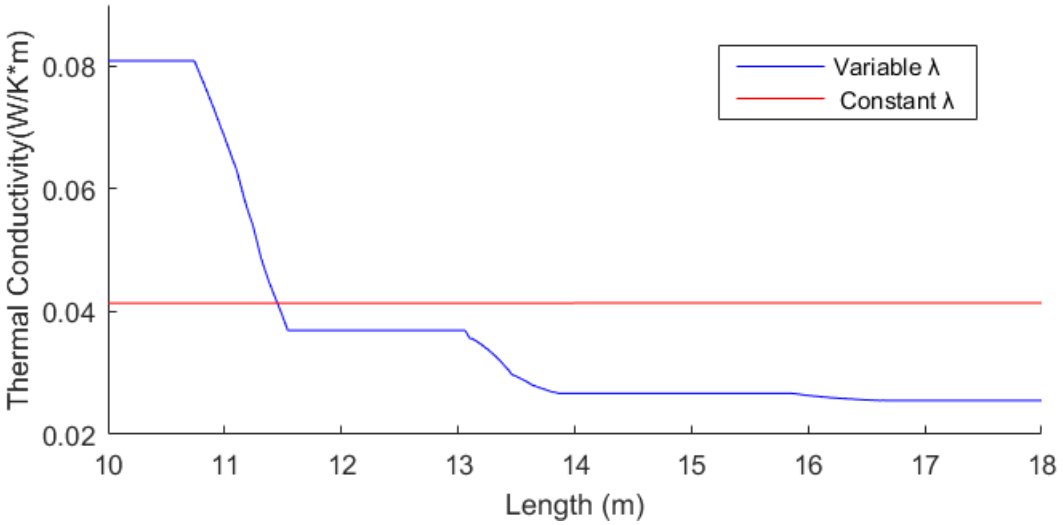

Figure 7.2: Bulk thermal conductivity throughout the core in the DeLight model. The blue line is the result of the 3^{rd} order spline and the red line the estimated value by Schenderling. On the vertical axis the thermal conductivity is displayed and the horizontal axis represents the location in the model.

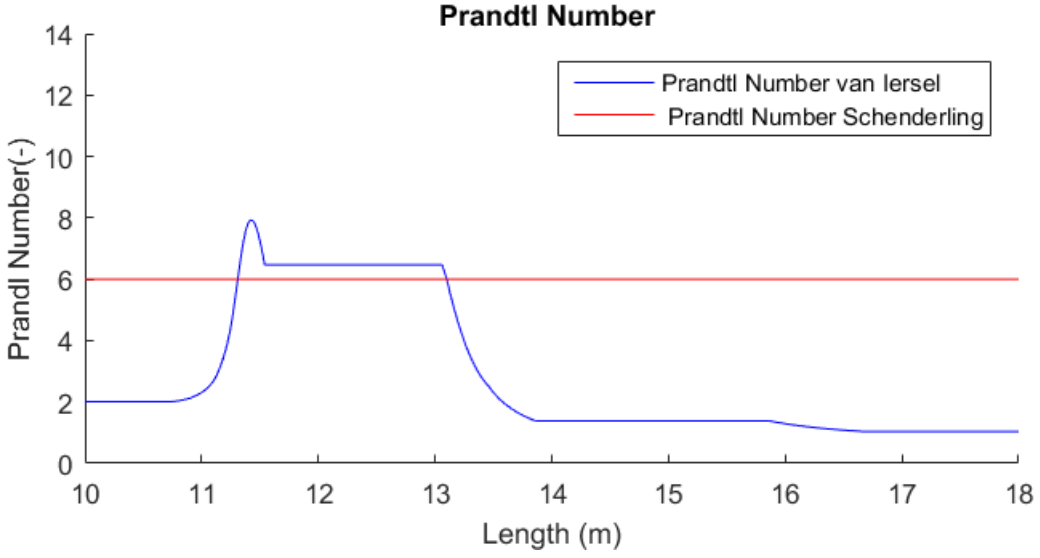

Figure 7.3: Bulk Prandtl number throughout the core in the DeLight model. The blue line is the newly calculated result and the red line the estimated value by Schenderling. On the vertical axis the Prandtl number is displayed and the horizontal axis represents the location in the model.

The next change in the model is the implementation of Mokry's Nusselt number correlation. A steady-state snap shot is taken(see figure 7.4) of the DeLight core using the new and old method to calculate the Nusselt number. Schenderling predicted a higher Nusselt

number in every core segment and thus better heat transfer from the tube wall to the bulk of the Freon. This behavior agrees with the prediction made in figure 6.7.

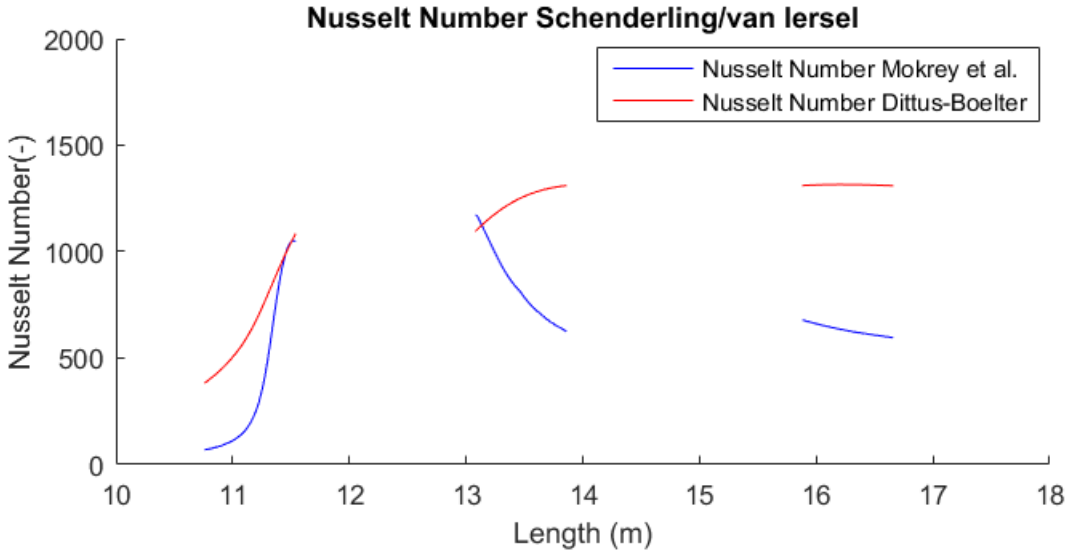

Figure 7.4: Nusselt number in each core section of the DeLight model. On the vertical axis the Nusselt number is displayed and the horizontal axis represents the location in the model. Note that this is not the correct implementation of Dittus-Boelter, see figure 6.7.

7.1.3 Mass-Flow Comparison

Here the effect of implementing the new correlations for heat transfer and the friction factor on steady-state mass-flow is assessed. First the new friction factor correlation and the heat loss to the environment are turned off, as they influence mass flow directly. This enables a comparison with the mass-flow as found by Spoelstra, see figure 7.5. This measurement is taken with a total core power set to $7,5kW$ and T_{inlet} at $0\,^{\circ}\mathrm{C}$. Although the start up mechanics are somewhat different, which can be attributed to the very different heat transfer dynamics, the flow rates converge beautifully as soon as a steady-state is reached. As expected, the adjusted heat transfer dynamics do no influence steady state mass flow.

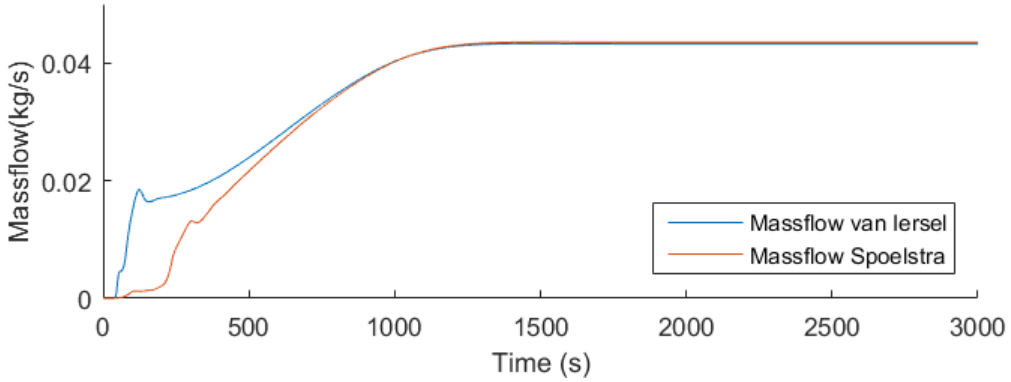

Figure 7.5: Mass-flow during the acquisition of steady-state in the DeLight model. On the vertical axis the mass-flow is displayed and the horizontal axis represents time in the model. Each time-step is one second.

Next, an attempt was made to reproduce the so-called power flow maps made by Spoelstra, now with the adjusted heat transfer model and friction factor correlation. The result(see figure 7.6) agree better or equally well with the experimental data. The $T_{inlet} = 0\,°C$ case is performed with preheater values equal to Spoelstra, i.e. 1250 W. This power is applied before the Freon enters the core, thus the temperature in the downcomer is lower than 0 °C, i.e. −19.9 °C. Where Spoelstra predicted a discontinuity in the power flow map, the adjusted model does not. Spoelstra concluded this discontinuity was caused by a yet unidentified physical aspect. The absence of this discontinuity can be attributed to the heat transfer and friction models.

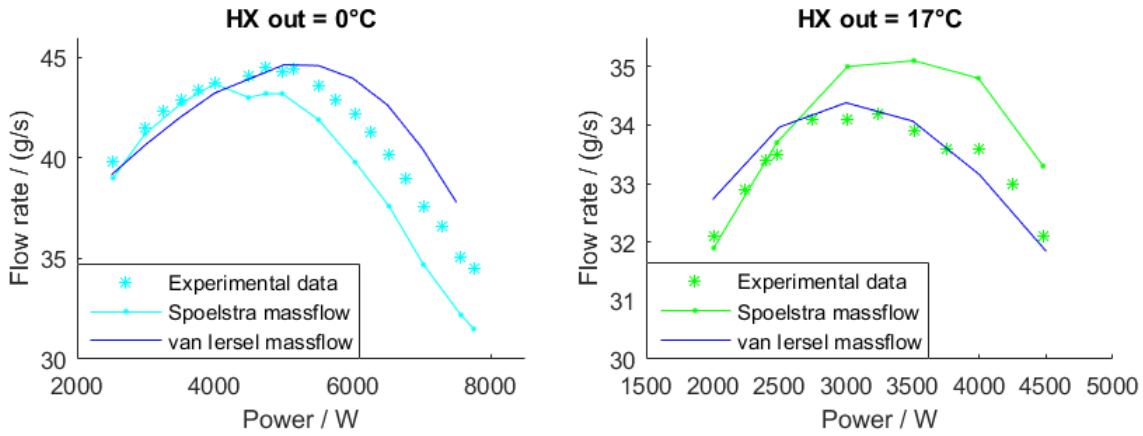

Figure 7.6: Power versus mass-flow plot, all measurements were done at steady-state. On the vertical axis the mass-flow is displayed and the horizontal axis represents the total power output by the three core segments.

7.2 Stability

7.2.1 Approximation of the Spoelstra NSB

To validate the new models, an attempt was made to reproduce the results found by Spoelstra, i.e. the neutral stability boundary, with the adjusted code. Spoelstra's measurements did not include a supercritical friction factor correlation, thermal inertia in the structure was not accounted for and heat flux was considered constant over each core segment. To approximate Spoelstra's neutral stability boundary, the new heat transfer model and fiction factor correlation are adjusted to approximate the models used by Spoelstra. For example, the supercritical effect of the new friction factor models is excluded, resulting in an isothermal friction factor correlation like the one used by Spoelstra. Also, the heat transfer dynamics are adjusted. The heat transfer dynamics are different from Spoelstra's model, equation (4.1), and are now dictated by equation (7.1).

$$\rho_{wall} C_{p,wall} V_{wall} \frac{dT_{wall}}{dt} = Q - \alpha_{in}(T_{wall} - T_{freon}) Per_{in} dz - \alpha_{out}(T_{wall} - T_{ambient}) Per_{out} dz \quad (7.1)$$

In order to obtain the constant heat flux required, the external heat transfer coefficient is modeled as 0 and the pre-set heat loss from Spoelstra's model is used again. Also, the internal heat coefficient is set to a constant value of 10^4, this is the same value Schenderling used in his successful approximation of Spoelstra's neutral stability boundary. Lastly, the

heat capacity and density of the Delight wall are set to a value close to zero. This will remove the effect of thermal inertia from the model. After these changes equation (7.1) approximated to equation (7.2).

$$T_{wall} - T_{freon} \approx Q \frac{1 - p_{loss}}{\alpha_{in} P_{in} dz} \tag{7.2}$$

The result of this approximation is shown in figure 7.7. The observed behavior matches the results of Spoelstra quite well. The slight deviations can be attributed to the adjusted heat transfer dynamics.

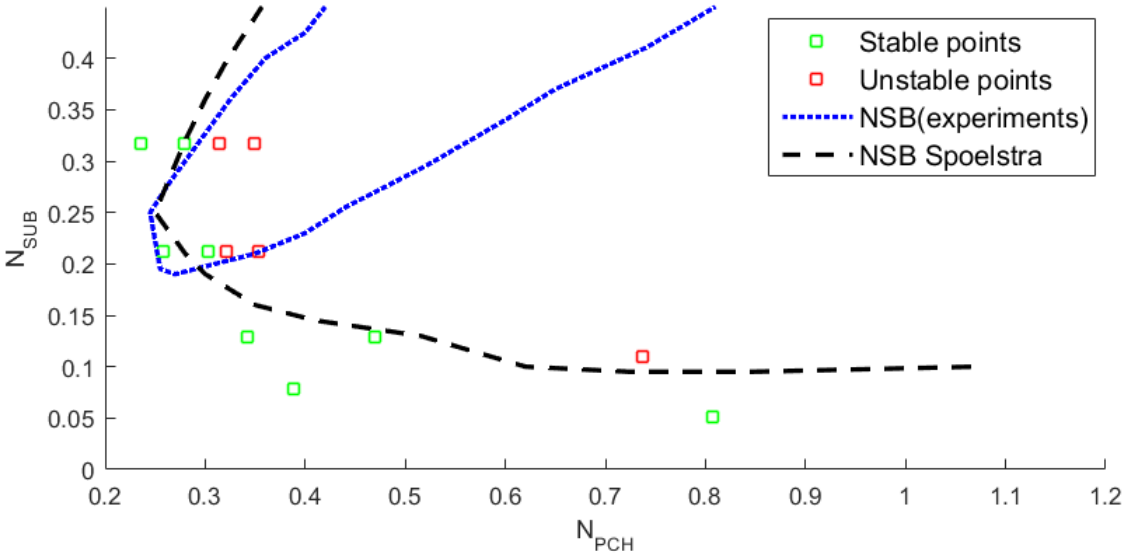

Figure 7.7: NSB as found by van Iersel and the stable/unstable data points. The NSB and data points are plotted in a dimensionless plane spanned by N_{PCH} and N_{SUB}.

7.2.2 Neutral Stability Boundary

A stability analysis with the advanced modeling for the friction factor and heat transfer dynamics yielded the neutral stability boundary as shown in figure 7.8. The squares represent either a stable(green) or unstable(red) working point. Each data point represents an individual calculation, with a steady-state as the initial condition, lasting for 50 seconds. The NSB closely approximates several points, this indicates a decay ratio near neutral value of $DR = 1$. In figure 7.9 the new neutral stability boundary is compared to Spoelstra's and Schenderling's neutral stability boundary as well as the experimental DeLight results, all for $\tau = 6$. The general behavior of the new NSB is similar to the experimental result and the study performed by Schenderling, the position within the dimensionless plane spanned by N_{PCH} and N_{SUB}, however, is not. The NSB seems to be shifted to the upper right, which is also observed by Schenderling. Although the shape of the NSB better approximates the behavior observed in the experimental results, it's clear the model does not accurately describe the stability within the DeLight facility. There are several types of errors made that could cause these deviations.

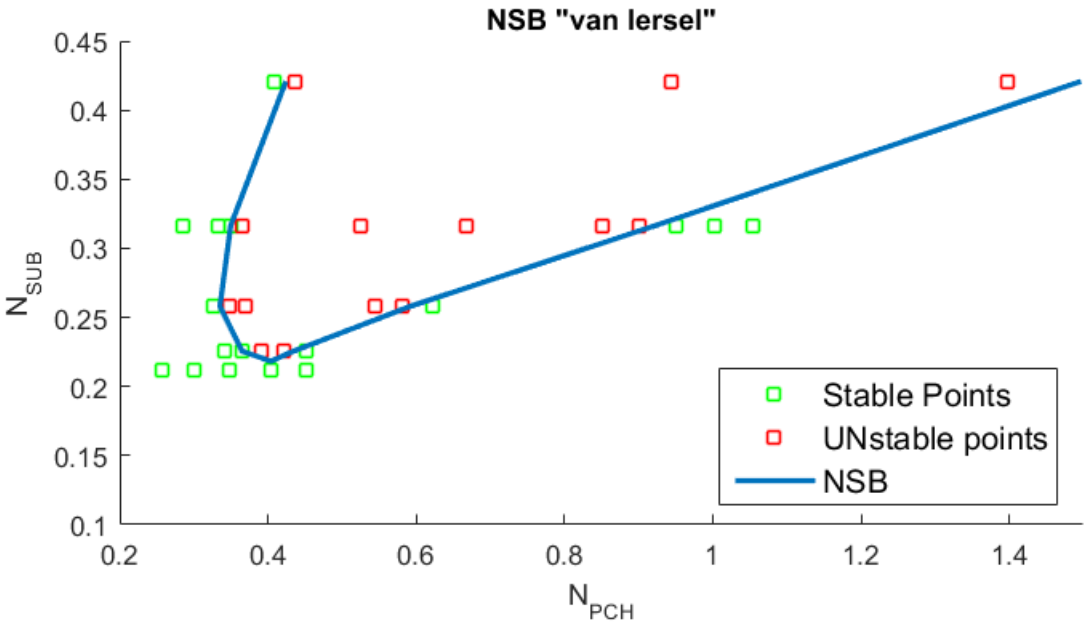

Figure 7.8: NSB as found by van Iersel and the stable/unstable data points. The NSB and data points are plotted in a dimensionless plane spanned by N_{PCH} and N_{SUB}.

First of all, Spoelstra(Spoelstra, 2012) concluded discretization errors can lead to numerical diffusion, which could still be a factor. However, this should only stabilize the system and thus can't explain the difference, at least not entirely. Additionally, several assumptions made in this thesis could cause the discrepancy.

Although more complex heat transfer modeling has been applied, its accuracy could still be debated. The literature concerning supercritical Nusselt correlations is contradictory and relatively inaccurate(Zahlan et al. 2010). Several data points have also been assessed with Bishop's correlation, which is fairly similar to Mokry, yet different decay ratios were obtained (see appendix C). Only three point where assess but all showed a higher decay ratio, about 10-25% higher, with only a small shift in N_{PCH}. Also, the external heat flux is simplified in the model, i.e. the Grashof number is averaged and only accounted for in the core and not in the rest of the facility.

The uncertainties concerning the supercritical Nusselt number also related to the supercritical friction factor model. Correlations found in literature do not agree well with each other and experimental data. All correlations have relatively large errors(Fang et al., 2012). Fang's correlation, however, performed well in the steady-state analysis, so this is unlikely to cause the discrepancy between model and measurements, unless small variations in the friction factor have a large impact on stability. When the isothermal friction factor is implemented instead of Fang et al., the decay ratio's seemed to increase slightly (see appendix D). Again, only a few calculations were conducted. The decay ratio's only changed 0-3.5%, which is much less than the case of the Nusselt number. The observed shifts in N_{PCH} where relatively small.

Lastly, it is possible that several physical phenomena are not yet identified in the DeLight model, causing the NSB to disagree with the model.

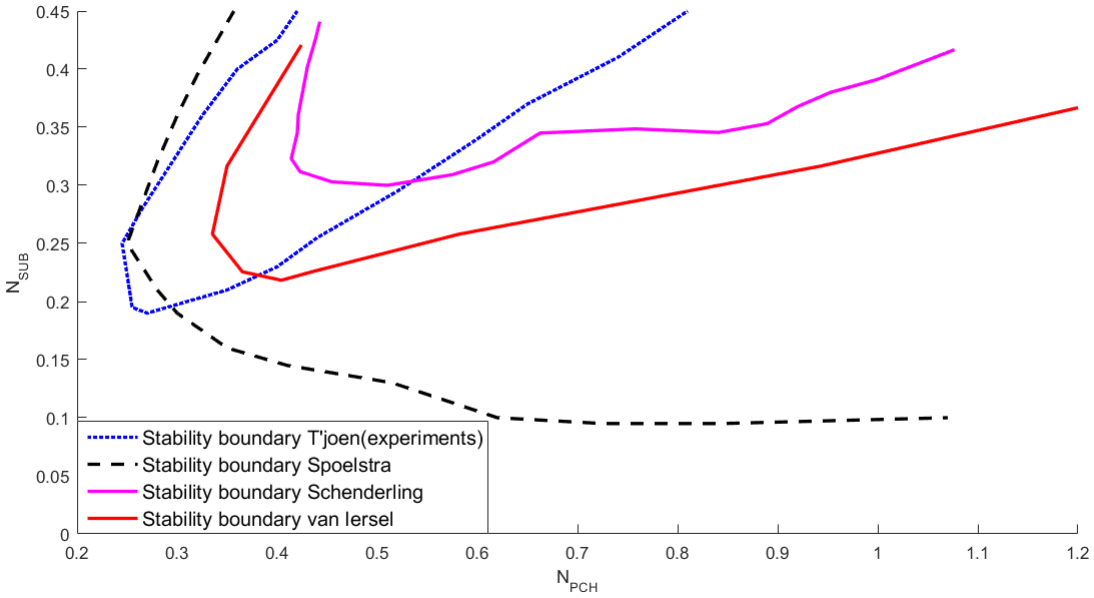

Figure 7.9: NSB as found by the experimental analysis as well as the computationally simulated NSB by Spoelstra, Schenderling and van Iersel. The NSB and data points are plotted in a dimensionless plane spanned by N_{PCH} and N_{SUB}.

Chapter 8

Conclusions

8.1 Conclusions

The aim of this thesis was to implement a supercritical friction factor correlations and heat transfer model in an excising numerical model of the DeLight facility to perform a stability analysis and to study the effect of the new correlations on the outcome of the numerical code. The friction factor correlation chosen was the one proposed by Fang(Fang et al., 2012). This correlation was implemented in the code and reduced the friction factor in all three core segments. Additionally, several changes were made to the heat transfer in the model. First, the initially constant value for the thermal conductivity was changes to a variable, using a spline. Second, the definition of the Prandtl number was implemented in the system which greatly changed its behavior throughout the model. The Prandtl number had also been assumed constant. Last, Mokry's Nusselt number correlation was used to more accurately describe the supercritical heat transfer in the model.

After these changes, power flow maps were produced that agreed similarly well or better with the experimental data than the results of Spoelstra. After the steady-state analysis the focus shifted to stability. To validate the adjusted code, the Spoelstra code was approximated. To achieve this, the new heat transfer model and fiction factor correlation were adjusted to approximate the models used by Spoelstra. The result matched the Spoelstra result with good accuracy. Finally a new neutral stability boundary was produced. Although the stability analysis yielded a neutral stability boundary that does not accurately describes the experimental findings, the approximation is better than both Spoelstra and Schenderling. The shape of the NSB's agreed fairly well but a shift to the upper right had taken place. Interestingly, it was found that the correlation used for the Nusselt number has a very large effect on the stability. The few assessed points showed a deviation between 10-25%, when Bishop(Bishop et al., 1965) was used instead of Mokry(Mokry et al., 2009). When at the same operating conditions only the isothermal friction term of the Fang correlation(Fang et al., 2012) was used only a small deviation was found(0-3,5%). Overall it can be concluded that the numerical model, that is the result of the adjustments done in this thesis, does not accurately describe the stability of the DeLight facility.

8.2 Outlook

The large difference between the computational stability prediction versus the experimental findings could be caused by numerical diffusion or a physical phenomena that is neglected(friction heat, axial heat conduction, etc.). However, it appears to be more likely caused by errors made with modeling the current physical phenomena. The neutral stability

boundary is highly depended on the current variables, such as the Nusselt number. The NBS found by Spoelstra, Schenderling and the one in this thesis are located very differently on the dimensionless plane spanned by N_{PCH} and N_{SUB}. Thus, the current modeling of the known phenomena is inadequate. For instance, the large deviation caused by different Nusselt number models is striking. The literature concerning these Nusselt correlations is contradictory and all correlations show relatively large errors. Because the Nusselt number has a significant influence on stability, it could improve the model if the effect of the Nusselt number on stability is qualitatively studied. The Nusselt number could also be experimentally investigated by measuring the wall temperature in the DeLight facility. Although the friction factor appears to have a much smaller effect on the NSB than the Nusselt number, it could be interesting to further investigate its effect on system stability as well. Both these suggestions could be part of a sensitivity analysis, which is something Spoelstra proposed in 2012. If it is known which parameters mainly influence stability, and how, a much better approximation of the experimental neutral stability boundary could be made.

Bibliography

[1] W. Ambrosini. *On the analogies in the dynamic behavior of heated channels with boiling and supercritical quids.* Nuclear Engineering and Design, 237(11):11641174, 2007.

[2] A.A. Bishop, R.O. Sandberg and L.S. Tong. *Forced Convection Heat Transfer to Water at Near-critical Temperatures and Supercritical Pressures* A.I.Ch.E.-I.Chem.E Symposium Series No. 2, pp. 7785, 1965.

[3] J.A. Boure, A.E. Bergles, and L.S. Tong. *Review of two-phase ow instability.* Nuclear Engineering and Design, 25(2):165192, 1973.

[4] F.W. Dittus and L.M.K. Boelter. *Publications on Engineering, Vol. 2, p. 443* 1930.

[5] X. Fang, Y. Xu, X. Su, and R. Shi. *Pressure drop and friction factor correlations of supercritical ow.* Nuclear Engineering and Design, 242:323330, 2012.

[6] K. Fukuda and T. Kobori. *Classication of two-phase ow instability by density wave oscillation model.* Journal of Nuclear Science and Technology, 16(2):95108, 1979.

[7] J. Hofmeister, C. Waata, J. Staringer, T. Schulenberg, and E. Laurien. *Fuel assembly design study for a reactor with supercritical water.* Nuclear Engineering and Design, 237(14): 15131521, 2007.

[8] J.D. Jackson. *Consideration of the heat transfer properties of supercritical pressure water in connection with the cooling of advanced nuclear reactors* Proceedings of the 13th Pacific Basin Nuclear Conference, 2002.

[9] F.A.L. Kam. *Development of a one-dimensional computer model for the stability analysis of a natural circulation super critical water reactor.* M.sc. thesis, Section Physics of Nuclear Reactors, Delft University of Technology, 2011.

[10] H.K. Koopman. *Development of the stealth-code and investigation of the eects of feedwater sparger positioning on the thermal-hydraulic stability of natural circulation boiling water reactors.* M.sc. thesis, Section Physics of Nuclear Reactors, Delft University of Technology, 2008.

[11] E.J. LeFevre and A.J. Ede. *Laminar Free Convection from the Outer Surface of a Vertical Circular Cylinder.* Proc. 9th International Congress on Applied Mechanics, Brussels, Vol. 4, pp. 175183, 1956.

[12] C.P. Marcel. *Experimental and Numerical Stability Investigations on Natural Circulation Boiling Water Reactors.* PhD thesis, Section Physics of Nuclear Reactors, Delft University of Technology, 2007.

[13] J. March-Leuba and J.M. Rey. *Coupled thermohydraulic-neutronic instabilities in boiling water nuclear reactors: a review of the state of the art.* Nuclear Engineering and Design, 145(1-2):97111, 1993.

[14] T. Ortega Gomez. *Stability analysis of the High Performance Light Water Reactor.* PhD thesis, Institute for Nuclear and Energy Technology, Karlsruhe Institute of Technology, 2009.

[15] S. Mokry, A. Farah, K. King, S. Gupta, I. Pioro and P. Kirillov. *Development of Supercritical Water Heat-Transfer Correlation for Vertical Bare Tubes.* Proceedings of the Nuclear Energy for New Europe 2009 International Conference, 2009.

[16] NERA website. URL: *http://www.nera.rst.tudelft.nl/fileadmin/Faculteit/TNW/Over-de-faculteit/Afdelingen/Radiation-Radionuclides-Reactors/Research/Research-Groups/NERA/ResearchProjects/img/DeLightNew.png*

[17] I. Pioro and S. Mokry *Heat Transfer to Supercritical Fluids, Heat Transfer - Theoretical Analysis, Experimental Investigations and Industrial Systems.* ISBN: 978-953-307-226-5, InTech, Available from: http://www.intechopen.com/books/heat-transfer-theoretical-analysis-experimentalinvestigations-and-industrial-systems/heat-transfer-to-supercritical-fluids, 2011

[18] V.N. Popov *Theoretical calculation of heat transfer and friction resistance for supercritical carbon dioxide.* Published as Rand report R-451-PR 1, 46-56.

[19] M. Rohde, C.P. Marcel, C. TJoen, A.G. Class, and T.H.J.J. Van Der Hagen. *Downscaling a supercritical water loop for experimental studies on system stability.* International Journal of Heat and Mass Transfer, 54(1-3):6574, 2011.

[20] T.K.F. Schenderling. *Numerical analysis of the inuence of wall thermal inertia on the stability of natural circulation driven supercritical water reactors.* B.sc. thesis, Section Physics of Nuclear Reactors, Delft University of Technology, 2008.

[21] T. Schulenberg, J. Staringer, and J. Heinecke. *Three pass core design proposal for a high performance light water reactor.* Progress in Nuclear Energy, 50(2-6):526531, 2008.

[22] J. Spoelstra. *Numerical stability analysis of natural circulation driven supercritical water reactors* M.sc. thesis, Section Physics of Nuclear Reactors, Delft University of Technology, 2008.

[23] C. TJoen and M. Rohde. *Experimental study of the coupled thermo-hydraulic-neutronic stability of a natural circulation HPLWR.* Nuclear Engineering and Design, 242:221232, 2012.

[24] N.E. Todreas and M.S. Kazimi. *Nuclear Systems 1.* Taylor & Francis, 1989

[25] R. Viswanathan, J.F. Henry, J. Tanzosh, G. Stanko, J. Shingledecker, B. Vitalis, and R. Purger *U.S. Program on Materials Technology for Ultra-Supercritical Coal Power Plants* Journal of Materials Engineering and Performance Volume 14(3) June 2005

[26] T. Yamashita, H. Mori, S. Yoshida, and M. Ohno. *Heat transfer and pressure drop of a supercritical pressure uid owing in a tube of small diameter.* Memoirs of the Faculty of Engineering, Kyushu University, 63(4):227244, 2003.

[27] H. Zahlan, D. Groeneveld, S. Tavoularis. *Look-Up Table for TransCritical Heat Transfer.* The 2nd Canada-China Joint Workshop on Supercritical Water-Cooled Reactors, 2010.

Appendices

Appendix A

Delight Technical Drawings

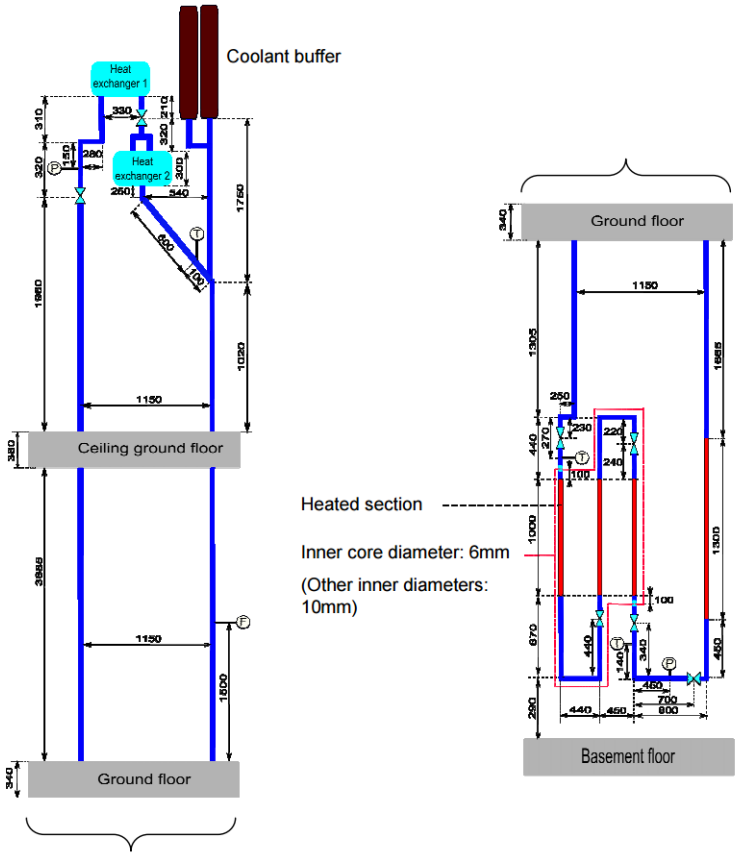

Figure A.1: Technical drawing of the delight facility. The goemetery of the components is indicated as well as the position of some sensors. The F indicates a flow meter, a T temperature measurement and P a pressure measurement.(source:)

Appendix B

Thermal Conductivity Spline

Thermal conductivity produced with added spline versus data from NIST. Good argeement is found.

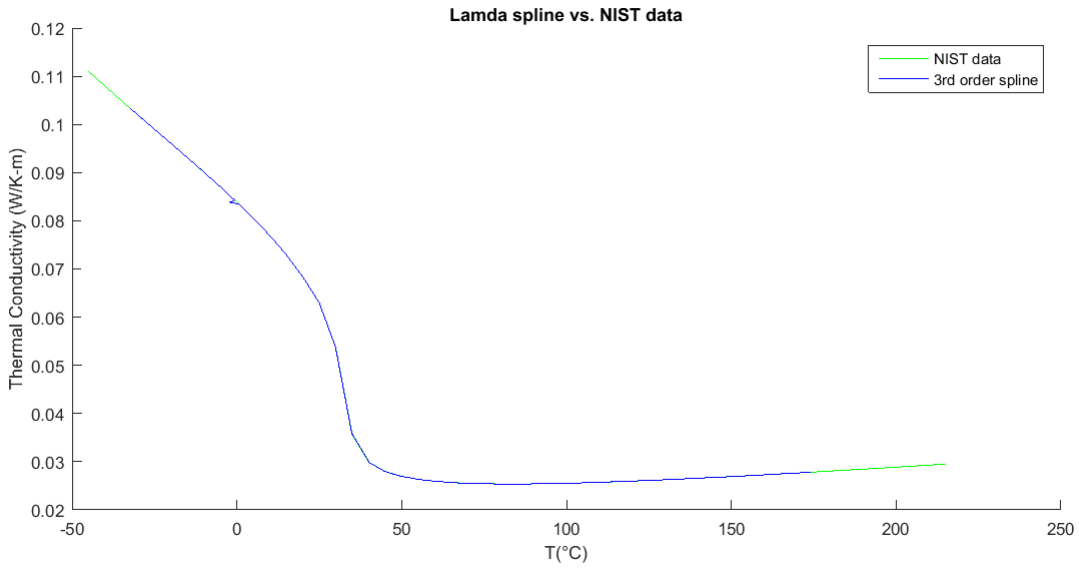

Figure B.1: 3rd Order spline plotted against NIST data.

Appendix C

Effect of Different Nusselt Correlation on Decay Ratio

Table C.1: Result of the use of a different Nusselt number correlation in same operating points.

Model	P_{Core}	T_{inlet}	N_{SUB}	N_{PHC}	DR
Mokry et al.	5000	−20 °C	0.4208	0.4083	**0.8823**
Bishop et al.	5000	−20 °C	0.4208	0.3990	**1.1639**
Mokry et al.	4000	0 °C	0.3166	0.3498	**0.9952**
Bishop et al.	4000	0 °C	0.3166	0.3466	**1.2318**
Mokry et al.	3750	15 °C	0.2256	0.3651	**0.9996**
Bishop et al.	3750	15 °C	0.2256	0.3661	**1.1264**

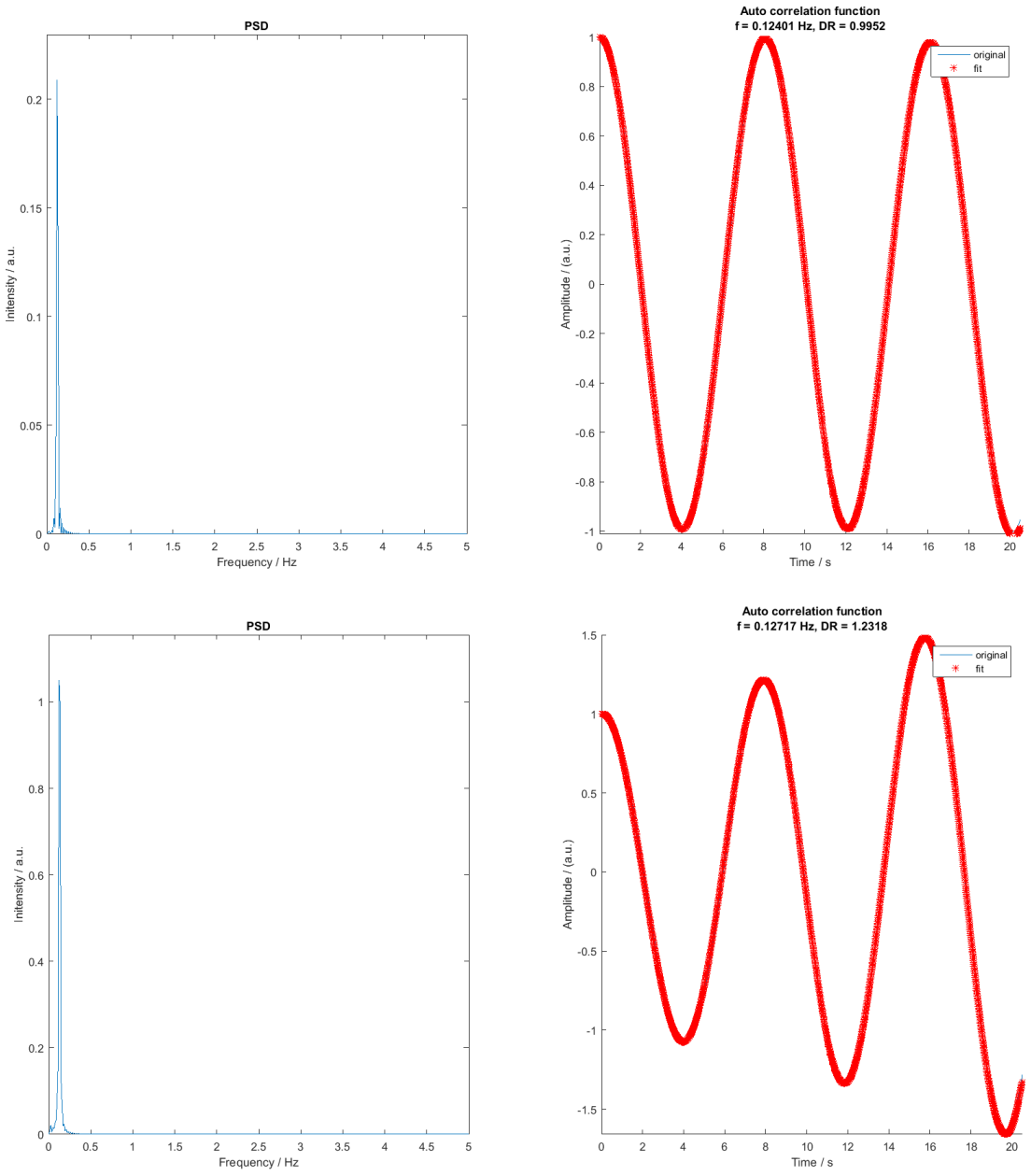

Figure C.1: Decay ration calculated with Mokry's Nusselt correlation(top) and bishop's Nusselt correlation(bottom). Both calculations where done op the same operating point with $T_{inlet} = 0\,°\mathrm{C}$ and core power set to $4kW$.

Appendix D

Effect of Different Friction Factor on Decay Ratio

Table D.1: Result of the use of a different friction factor correlation in same operating points.

Model	P_{Core}	T_{inlet}	N_{SUB}	N_{PHC}	DR
Fang et al.	5000	−20 °C	0.4208	0.4083	**0.8823**
Isothermal	5000	−20 °C	0.4208	0.4140	**0.9223**
Fang et al.	4000	0 °C	0.3166	0.3498	**0.9952**
Isothermal	4000	0 °C	0.3166	0.3545	**1.0296**
Fang et al.	5750	10 °C	0.258	0.5819	**1.0067**
Isothermal	5750	10 °C	0.258	0.5845	**0.9821**
Fang et al.	3750	15 °C	0.2256	0.3651	**0.9996**
Isothermal	3750	15 °C	0.2256	0.3681	**0.9918**

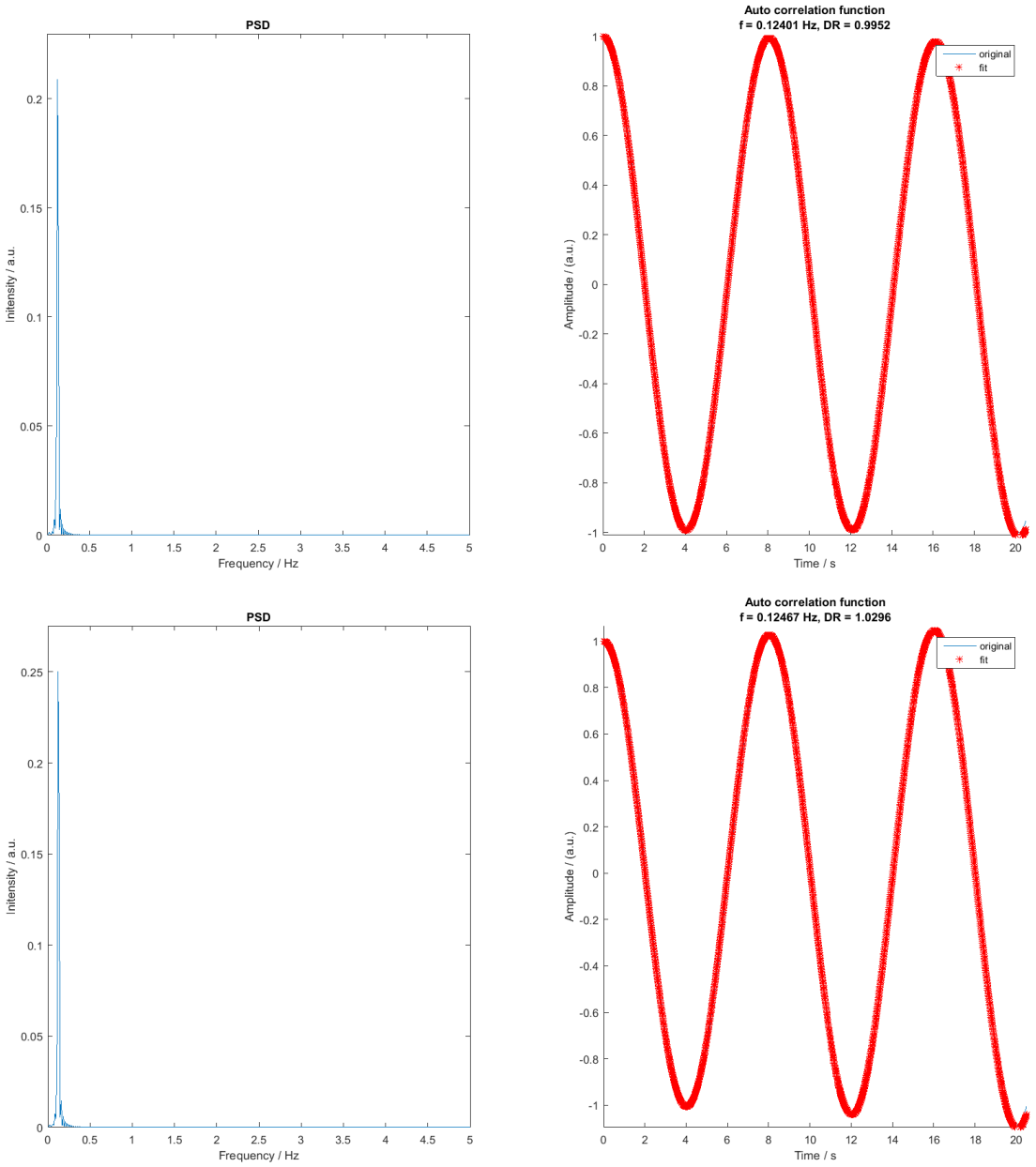

Figure D.1: Decay ration calculated with Fang's friction factor correlation(top) and only the isothermal part of the correlation(bottom). Both calculations where done op the same operating point with $T_{inlet} = 0\,°C$ and core power set to $4kW$.

List of Figures

List of Tables

Nomenclature

Symbol	Dimensions	Description
Roman Symbols		
D	m	Diameter
M	kg/s	Mass-flow
A	m^2	Surface area
f	(-)	Darcy-Weisbach friction factor
Q'	W/m	Linear heating rate
Q''	W/m^2	Surface heating rate
P	W	Power
Per	m	Perimeter
C_p	J/K	Heat Capacity
V	m^3	Volume
g	m/s^2	Gravitational constant
x	m	Distance to core inlet point(Bishop)
n	(-)	Variable(Jackson)
Greek Symbols		
τ	s	Time constant
ϵ	m	Absolute wall roughness
$\tilde{\tau}$	kg/ms^2	Shear stress
ρ	kg/m^3	Density
μ	kg/ms	viscosity
α	W/Km^2	Heat transfer coefficient
λ	W/Km	Thermal Conductivity
β	$1/K$	Volumetric thermal expansion coefficient

ν	m^2/s	Kinematic viscosity
θ	(-)	Constant value between 1 and 0

Subscripts		
b		Bulk property
w		Wall property
pc		Property at pseudo-critical point
f		Darcy-Weisbach friction factor
iso		Isothermal
tot		Total
avg		Average value
H		Hydraulic
J		Jackson
B		Bishop
M		Mokry

Dimensionless		
Re	(-)	$Re = \frac{MD}{A\mu}$
N_{SUB}	(-)	$N_{SUB} = \frac{h_{pc}-h_{in}}{h_{pc}}$
N_{PCH}	(-)	$N_{PCH} = \frac{P_{core}}{Mh_{pc}}$
Nu	(-)	Nusselt Number(several definitions used)
Pr	(-)	$Pr = \frac{\mu C_p}{\lambda}$
Gr	(-)	$Gr = \frac{g\beta(T_{wall}-T_{ambient})D^3}{\nu^2}$

Acronyms	
BWR	Boiling Water Reactor
PWR	Pressurized Water Reactor
DeLight	Delft Light Water Reactor
DWO	Density Wave Osculation
LWR	Light Water Reactor
HPLWR	High Performance Light Water Reactor
NSB	Neutral Stability Boundary

SCWR	Super Critical Water Reactor
PNR	Physics of Nulear Reactors